© 2014. Published by The Company of Biologists Ltd | Development (2014) 141, 563-573 doi:10.1242/dev.097022

RESEARCH ARTICLE

Endophilin B is required for the *Drosophila* oocyte to endocytose yolk downstream of Oskar

Yi-Cheng Tsai[1,*], Wei Chiang[1,*], Willisa Liou[2], Wei-Hao Lee[1], Yu-Wei Chang[1], Pei-Yu Wang[3,4], Yi-Chen Li[1], Tsubasa Tanaka[5], Akira Nakamura[5] and Li-Mei Pai[1,3,4,‡]

ABSTRACT

The nutritional environment is crucial for *Drosophila* oogenesis in terms of controlling hormonal conditions that regulate yolk production and the progress of vitellogenesis. Here, we discovered that *Drosophila* Endophilin B (D-EndoB), a member of the endophilin family, is required for yolk endocytosis as it regulates membrane dynamics in developing egg chambers. Loss of D-EndoB leads to yolk content reduction, similar to that seen in *yolkless* mutants, and also causes poor fecundity. In addition, mutant egg chambers exhibit an arrest at the previtellogenic stage. D-EndoB displayed a crescent localization at the oocyte posterior pole in an Oskar-dependent manner; however, it did not contribute to pole plasm assembly. D-EndoB was found to partially colocalize with Long Oskar and Yolkless at the endocytic membranes in ultrastructure analysis. Using an FM4-64 dye incorporation assay, D-EndoB was also found to promote endocytosis in the oocyte. When expressing the full-length *D-endoB*^{FL} or *D-endoB*$^{\Delta SH3}$ mutant transgenes in oocytes, the blockage of vitellogenesis and the defect in fecundity in *D-endoB* mutants was restored. By contrast, a truncated N-BAR domain of the D-EndoB only partially rescued these defects. Taken together, these results allow us to conclude that D-EndoB contributes to the endocytic activity downstream of Oskar by facilitating membrane dynamics through its N-BAR domain in the yolk uptake process, thereby leading to normal progression of vitellogenesis.

KEY WORDS: Endophilin B, Oskar, Vitellogenesis, Yolk protein, Fecundity, *Drosophila*

INTRODUCTION

In *Drosophila melanogaster*, a nutritional environment modulates hormonal conditions to regulate oogenesis through yolk protein synthesis and the progression of vitellogenesis (Bownes et al., 1988; Compagnon et al., 2009; Drummond-Barbosa and Spradling, 2001; Tufail and Takeda, 2009). Yolk proteins are the sole nutritional source for *Drosophila* embryogenesis. They are synthesized in follicle cells and fat bodies, and are taken up by the oocytes through endocytosis during *Drosophila* oogenesis (Compagnon et al., 2009; Morrison et al., 2008; Richard et al., 2001). *Drosophila* oogenesis can be divided into 14 stages involving a process of egg chamber growth and maturation. The germline of 15 nurse cells and one oocyte are surrounded by a single-layered follicle cell epithelium. Yolk proteins are synthesized in the somatic follicle cells from stage 8 onwards, which is the beginning of vitellogenesis (Brennan et al., 1982). The yolk protein receptor Yolkless, which belongs to the low density lipoprotein receptor (LDLR) family, transports the yolk protein into oocytes through clathrin-dependent endocytosis and is recycled back to the membrane through tubular membrane structures (Schonbaum et al., 1995; Schonbaum et al., 2000; Sommer et al., 2005). Even though several endocytic components are known to be required for endocytosis in the oocyte, the process of yolk endocytosis is not completely understood.

Oskar protein is spatially restricted to the posterior pole of the oocyte by transport, asymmetric anchorage, and local translation of *oskar* mRNA (Riechmann and Ephrussi, 2001). *oskar* mRNA encodes two protein isoforms, which perform different functions in pole plasm assembly and are localized to different subcellular structures. Short Oskar is concentrated in the polar granules where it recruits *vasa*, *tudor* and *nanos* for assembling the pole plasm (Breitwieser et al., 1996; Markussen et al., 1995; Vanzo et al., 2007; Vanzo and Ephrussi, 2002). Long Oskar is localized at the endocytic membrane and is required for anchoring the pole plasm (Vanzo et al., 2007; Vanzo and Ephrussi, 2002). Recently, the role of Long Oskar in the yolk endocytosis and the F-actin projection at the posterior pole were found (Vanzo et al., 2007). Rab5 and its effector protein, Rbsn5, are also involved in yolk endocytosis (Compagnon et al., 2009; Morrison et al., 2008). Rbsn5 acts downstream of Long Oskar for the pole plasm and endosomal protein anchorage (Tanaka and Nakamura, 2008). Furthermore, downstream of the Long Oskar regulated endocytic pathway, a Golgi-endosomal protein, Mon2, regulates the Capu-Spir-Rho1 complex to promote F-actin projections for pole plasm anchoring (Tanaka et al., 2011). Although Oskar-regulated pole plasm assembly has been well studied, it is still unclear how Oskar regulates yolk content.

The endophilin family proteins were first identified in the search for SH3 domain-containing proteins (Micheva et al., 1997). All endophilins contain the N-BAR (Bin-Amphiphysin-Rvs) and SH3 (Src-homology 3) domains. The N-BAR domain contributes to membrane binding and bending, and the SH3 domain interacts with proteins containing a proline-rich domain (Ringstad et al., 1997; Simpson et al., 1999; Sundborger et al., 2011). Endophilin family proteins bind to the membrane to drive the membrane curvature in two distinct ways (Dawson et al., 2006; Masuda et al., 2006; Peter et al., 2004). First, the N-BAR domain senses and binds to already bent membranes. Second, the N-BAR domain can directly induce the flat membrane curvature for its own association. Insertion of two amphipathic helices in the N-BAR, H0 and H1I, promote membrane curvature, and the BAR main body dimerization stabilizes the endophilin protein on the membrane. Finally, two SH3 domains are exposed and allow other

[1]Graduate Institute of Biomedical Sciences, College of Medicine, Chang Gung University, Tao-Yuan, 333, Taiwan. [2]Department of Anatomy, College of Medicine, Chang Gung University, Tao-Yuan, 333, Taiwan. [3]Department of Biochemistry, College of Medicine, Chang Gung University, Tao-Yuan, 333, Taiwan. [4]Chang Gung Molecular Medicine Research Center, College of Medicine, Chang Gung University, Tao-Yuan, 333, Taiwan. [5]Department of Germline Development, Division of Organogenesis, Institute of Molecular Embryology and Genetics, Kumamoto University 2-2-1 Honjo, Kumamoto 860-0811, Japan.
*These authors contributed equally to this work

‡Author for correspondence (pai@mail.cgu.edu.tw)

Received 12 April 2013; Accepted 31 October 2013

Development (2014) doi:10.1242/dev.097022

endocytic components to interact with endophilin proteins (Gallop et al., 2006).

Endophilin B is thought to be involved in membrane dynamic processes. Human endophilin B1 (SH3GLB1; also called Bif-1) is required for the maintenance of mitochondrial morphology (Karbowski et al., 2004). Endophilin B1 partially localizes to the Golgi complex and deforms lipid bilayers into tubules in an *in vitro* assay (Farsad et al., 2001). Moreover, endophilin B1 is colocalized with COPI (coat protein I), which is a protein complex involved in retrograde transport, and is required for COPI-vesicle formation (Yang et al., 2006). Recently, endophilin B1 has been found to play a role in autophagosome formation by protein-protein interaction through its SH3 domain (Takahashi et al., 2007; Takahashi et al., 2011; Takahashi et al., 2008; Takahashi et al., 2009). Here, we report that *Drosophila* Endophilin B (D-EndoB; EndoB – FlyBase) participates in Oskar-dependent endocytosis that affects the yolk content of the oocyte. We also show that lack of D-EndoB leads to reduced egg production. Moreover, we found that the N-BAR domain of D-EndoB alone was sufficient for promoting endocytosis, whereas the SH3 domain was dispensable.

RESULTS

Identification of Endophilin B in *Drosophila*

To reveal the function of Endophilin B (*CG9834*) in *Drosophila*, we first generated the D-EndoB protein null mutant by P-element imprecise excision. *endoB*^{EY00696} contains one P-element insertion at the 30th nucleotide away from *D-endoB 5′ UTR*. From 200 excision lines with PCR screening, we identified a protein null allele, *D-endoB*^{54}, which contains a large deletion region of 325 amino acids from the N-terminus that includes the whole N-BAR domain and a part of the SH3 domain, as shown in Fig. 1A. We next generated a polyclonal antibody against D-EndoB and tested its specificity by western blotting (Fig. 1B). We detected a band migrating just underneath the 43-kDa marker. This is consistent with the 42.3 kDa molecular weight predicted from the protein sequence (by Expasy-Compute pI/MW). Moreover, this band was only detected in wild-type ovaries but not in *D-endoB*^{54} homozygous ovaries, nor in the *D-endoB*^{54}*/Df(2R)BSC26* hemizygous ovaries (Fig. 1B). Interestingly, when analyzing whole protein extract of wild-type females, we detected an extra band at a molecular weight (Fig. 1C, arrowhead, lane 1) higher than the predicted 42.3 kDa (Fig. 1C, arrow); however, this band was entirely absent in the mutant females. Therefore, the possibility of non-specific recognition of anti-D-EndoB antibody can be eliminated. To test whether this unexpected band was from non-ovarian tissues, we further analyzed the ovariectomized females. We found that the predicted 42.3 kDa of D-EndoB only existed in wild-type females but not in *D-endoB*^{54} mutant females nor in females in which the ovaries had been removed (Fig. 1C, arrow), indicating that this 42.3 kDa isoform is mainly expressed in the ovary and that the other isoform is present in other tissues. Even though the anti-D-EndoB antibody was raised to recognize D-EndoB-PB, which is encoded by a *D-endoB* cDNA-PB derived from ovarian cDNA library, this antibody seemed to recognize the other isoform, D-EndoB-PA, which contains an extra

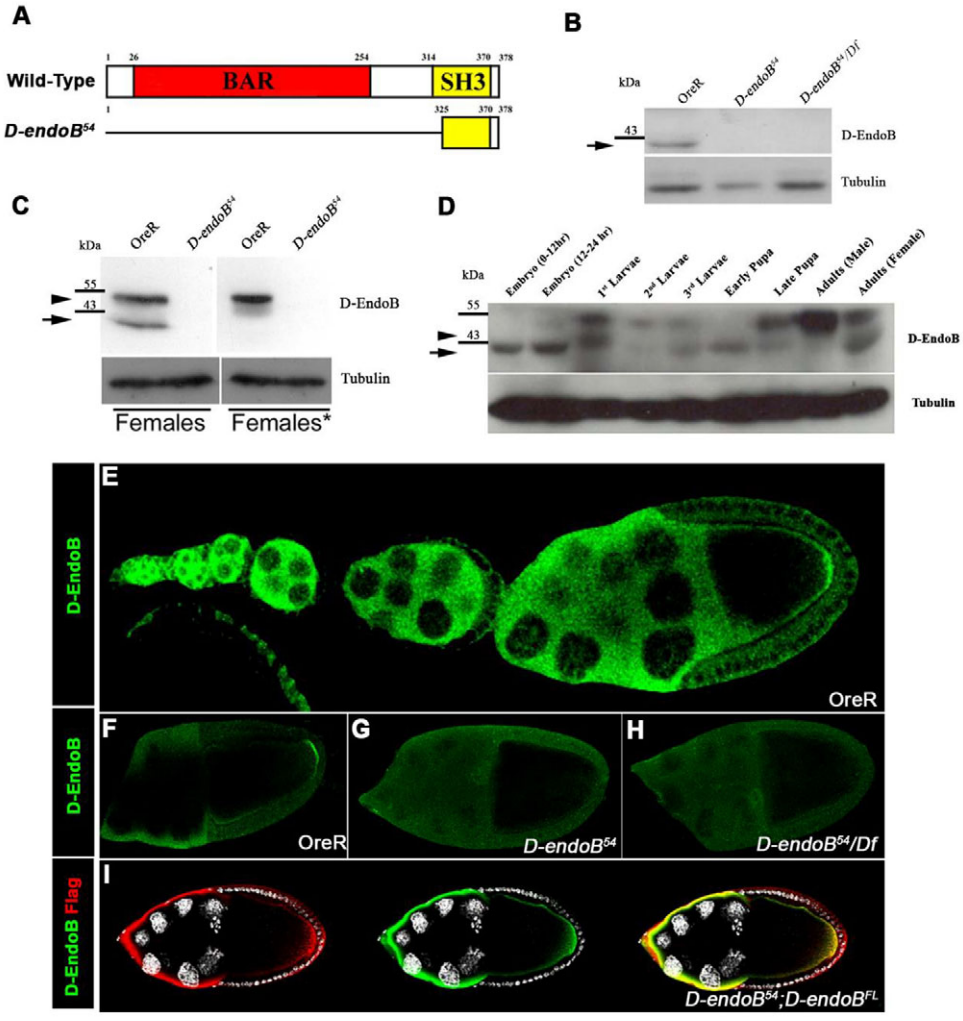

Fig. 1. The expression profiles of Endophilin B in *Drosophila*. (A) The wild-type *Drosophila* Endophilin B consists of two conserved domains. The N-BAR domain (red, amino acids 26-254) and the SH3 domain (yellow, amino acids 314-370). *D-endoB*^{54} is a protein null allele. (B) Western blot analysis of ovaries from wild-type and *D-endoB* null flies. The arrow indicates a band consistent with the predicted size of D-EndoB at 42.3 kDa. (C) Immunoblotting analysis of total fly extracts. A higher molecular weight isoform of *D-endoB* was detected only in the ovary-excluded female (asterisk indicates ovariectomized females). (D) Detection of the protein extracts from *Drosophila* developmental stages with anti-D-EndoB (top) and anti-α-Tubulin (bottom) antibodies. (E-H) D-EndoB (green) could be detected in the germline nurse cell since early oogenesis and was localized at the oocyte posterior at middle stage 9 (E). At middle stage 10, D-EndoB was strongly enriched at the posterior pole of the oocyte (*n*=17/21; F) compared with *D-endoB*^{54} homozygous (*n*=18/18; G) and *D-endoB*^{54}*/Df(2R)BSC26* hemizygous (*n*=19/19; H) egg chambers. (I) Distribution of the ectopic expressed D-EndoBFL in *D-endoB* null mutant background (*n*=20/24) was detected by anti-D-EndoB (green) and anti-Flag (red) antibodies. DAPI (white) staining indicates the nucleus.

Development (2014) doi:10.1242/dev.097022

12 amino acids (Fig. 1C). Analysis of D-EndoB expression through different developmental stages revealed that the PB form of D-EndoB is the only isoform in embryonic stages and is not present in the adult male (Fig. 1D), which suggests that only the ovary expresses D-EndoB-PB and contributes this isoform to the embryo. Our study focused on the function of D-EndoB-PB.

To determine the expression pattern of ovary-specific D-EndoB during oogenesis, D-EndoB localization in wild-type egg chambers was detected by immunofluorescence staining. D-EndoB expression could be detected mainly in germline nurse cells beginning in early oogenesis (Fig. 1E), and no expression was detected in somatic follicle cells in mosaic mutant clone analysis (supplementary material Fig. S1A,B). During stage 9 to 10A, D-EndoB displayed an enriched crescent-shaped pattern at the posterior pole in the oocyte (Fig. 1E; supplementary material Fig. S2), which is reminiscent of the localization of proteins of the posterior group, including Oskar, Vasa and Staufen. The localization of *D-endoB* mRNA in the ovary did not show a similar pattern (supplementary material Fig. S1C,D). This specific localization was confirmed by comparing the *D-endoB* null ovaries at stage 10 (Fig. 1F-H) and the exogenous expression of the Flag-tagged *D-endoB-PB* employing the germline-specific *UASp/GAL4* system (Fig. 1I; supplementary material Fig. S3) (Rørth, 1998). Our finding demonstrates that D-EndoB expresses in the germline cells and displays a unique crescent-shaped localization in the posterior of *Drosophila* oocytes.

D-EndoB affects the yolk content in the oocyte and the fecundity of female flies

We found that loss of D-EndoB led to fewer surviving offspring in the *D-endoB*^{54} mutant stock, and there was ~20% lethality of *D-endoB*^{54} mutant. To measure the fecundity of mutant females, newly eclosed females of specific genotypes were crossed with wild-type males. The numbers of eggs laid and hatched were counted every 24 hours for 4 days. We found that a single OreR female laid ~71 eggs per day; by contrast, *D-endoB*^{54} mutant females laid fewer eggs (Fig. 2A; ~47 eggs/day), and this was also true for *oskar* females (Fig. 2A; ~57 eggs/day). Similarly, the control of the *D-endoB*^{54}*/Df(2R)BSC26* hemizygous mutant females also showed a low level of egg production (Fig. 2B). The hatching rate of embryos was not affected in the absence of D-EndoB. When ectopically expressing the full-length *D-endoB* transgene *D-endoB*^{FL} in the *D-endoB* mutant background, the fecundity defect could be restored (Fig. 2B). Moreover, in transgenic lines with different expression levels of *D-endoB*^{FL} (supplementary material Fig. S3A, line #10 and line #4 express high and low level of D-EndoB-PB, respectively), the rescue ability showed a dosage-dependent effect (Fig. 2B). In conclusion, *D-endoB*^{54} mutant females exhibit a fecundity defect as the egg production is reduced.

Egg production and fertility are directly affected by yolk content in the oocyte during oogenesis (Bownes et al., 1988). We therefore investigated whether the yolk content is altered in the *D-endoB*^{54} mutant oocyte by examining the yolk accumulation of stage 9 oocytes in both wild type and *D-endoB* null mutants. As shown in Fig. 2C, the yolk spheres, ranging from ~0.2 to ~2.5 μm in diameter, were distributed evenly throughout the wild-type ooplasm. However, in *D-endoB* mutant oocytes (Fig. 2D), the density of yolk granules was dramatically decreased in the center of the oocyte, which is similar to the phenotype of the *yolkless* mutant oocyte (DiMario and Mahowald, 1987). As a result, a yolk-dense cortical zone and a yolk-space central zone could be easily distinguished at low magnification.

To quantify the differences in the yolk sphere, we performed a morphometric analysis on electron micrographs. The following three

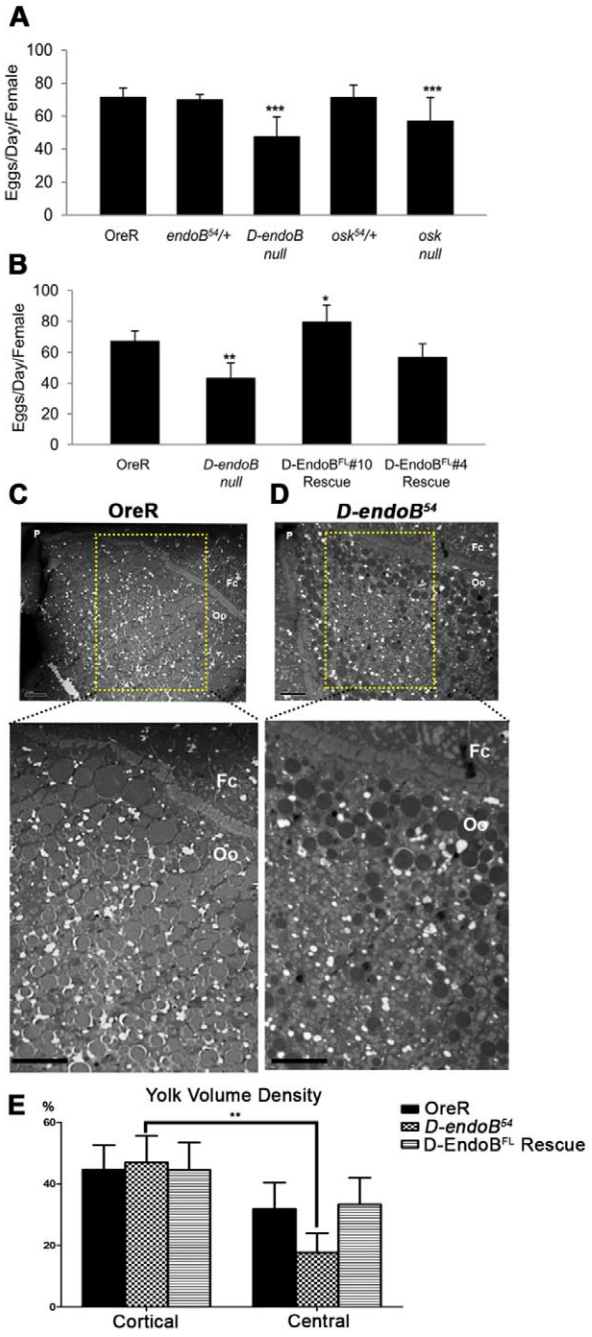

Fig. 2. The accumulation of yolk and fecundity are impaired in the *D-endoB* mutant. (A) Eggs produced by OreR females (mean ± s.d.; *n*=11), *D-endoB*^{54}/+ females (mean ± s.d.; *n*=11), *D-endoB*^{54} homozygous, *osk*^{54}/+ (mean ± s.d.; *n*=11) and *osk*^{54}*/Df(3R)p*^{XT103} (mean ± s.d.; *n*=20) mutant females. ***P<0.001. (B) Eggs produced by OreR females, *D-endoB54/Df(2R)BSC26*, and two rescued females: D-EndoBFL #10, and D-EndoBFL #4. (Analyses of these four genotypes, mean ± s.d.; *n*=6 in three individual experiments.) *P<0.05; **P<0.01. (C-E) Analysis of yolk granule distribution in mid-plane sections of late stage 9 egg chambers. In the wild-type flies (C), yolk granules are seen fairly evenly distributed throughout the ooplasm. In the *D-endoB* mutant (D), the density of yolk granules are greatly reduced in the central ooplasm. Scale bars: 10 μm. (E) Quantitative analysis of yolk volume density. Note that the discrepancy of yolk distribution at cortical and central regions can be corrected in *rescued-D-endoB* strain. **P<0.005. Total areas quantified were 1134 μm^2 (OreR, *n*=7), 1354 μm^2 (*D-endoB*^{54}, *n*=8) and 1050.6 μm^2 (D-EndoB^{FL} rescue, *n*=9) for the cortical zone and 775.8 μm^2 (OreR), 508 μm^2 (*D-endoB*^{54}) and 786.9 μm^2 (D-EndoB^{FL} rescue) for the central zone, respectively.

Development (2014) doi:10.1242/dev.097022

groups of strains were included: the wild type, the *D-endoB*^{54} null allele and an exogenous *D-endoB*-rescued genotype. The volume densities of yolk spheres at the cortical zone were similar in each group (averaged ~44-46%), whereas the volume density in the central region differed among the groups (Fig. 2E). This defect did not result from a reduction of yolk protein as the amount of yolk protein in the mutant ovary was not altered (supplementary material Fig. S4).

Localization of D-EndoB depends on the oocyte polarity

The anteroposterior polarity of the *Drosophila* oocyte is initially established by Gurken localization around stage 7 of oogenesis, following the remodeling of the microtubule arrays that is necessary for the polarized localization of *oskar* and *bicoid* mRNA (Nilson and Schüpbach, 1999). To test whether the posterior localization of D-EndoB depends on oocyte polarity, we assayed D-EndoB localization in *gurken* null mutant oocytes. In stage 9 egg chambers, Gurken was detected at the oocyte dorsal-anterior corner and D-EndoB was enriched at the posterior pole (Fig. 3A). In *gurken* null oocytes, D-EndoB was diffused towards the center of the oocytes (Fig. 3B), suggesting that the correct oocyte polarity is necessary for the localization of D-EndoB. To further confirm the requirement of cell polarity for the localization of D-EndoB, we treated ovaries with colcemid, which disrupts the microtubule and affects the cell polarity, and found that the Gurken was mislocalized and D-EndoB was diffuse (Fig. 3C). Taken together, it can be concluded that posterior localization of D-EndoB requires the correct establishment of polarity in the oocyte.

D-EndoB is recruited by the Long form of Oskar in the oocyte

Because of the posterior localization of D-EndoB, Oskar and Vasa (Fig. 3D,G,J), we examined if the localization of D-EndoB depends on Oskar. The absence of Vasa in the oocyte caused only slight alteration in the localization of D-EndoB (Fig. 3K; supplementary material Fig. S2), whereas D-EndoB was mislocalized in the absence of Oskar (Fig. 3L; supplementary material Fig. S2). The slight effect of *vasa* on D-EndoB localization could be explained by the feedback regulation of *vasa* on the translation of *oskar* (Markussen et al., 1997; Markussen et al., 1995). In the *D-endoB*^{54} mutant oocyte, the localization of Oskar and Vasa were not affected (Fig. 3F,I). The pole cell number in the embryos produced by *D-endoB* mutant females was not significantly changed (supplementary material Fig. S5). These results suggest that although D-EndoB is one member of the Oskar downstream components recruited to the posterior, it is not involved in pole plasm assembly.

To investigate further whether Oskar contributes to the localization of D-EndoB, we examined the localization of D-EndoB via expression of an *osk-bcd3'UTR* transgene, which ectopically localizes Oskar at the anterior of the oocyte (Fig. 4A). Associated with the ectopic expression of *osk-bcd3'UTR*, D-EndoB intensively accumulated at the anterior cortex of the oocyte (Fig. 4D), indicating that Oskar protein controls the localization of D-EndoB. Because of the functional diversity of the two Oskar isoforms, we wondered whether the D-EndoB localization depended specifically on one of the Oskar isoforms. When Long Oskar was expressed in the anterior oocyte (Fig. 4B), D-EndoB became detectable at ectopic sites (Fig. 4E). By contrast, the anteriorly expressed Short Oskar (Fig. 4C) could not recruit D-EndoB significantly (Fig. 4F). To eliminate the possibility that the ectopically expressed Oskar transgenes enhance the total protein level of the D-EndoB leading to this ectopic localization, we tested the D-EndoB expression and found no significant changes in protein levels (supplementary material Fig. S3B). These data indicate that Long Oskar, but not Short Oskar, determines the localization of D-EndoB.

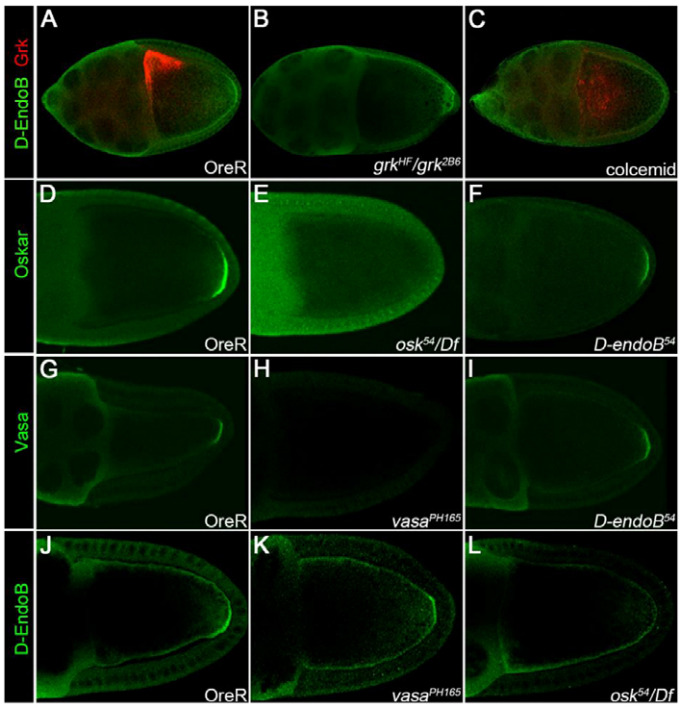

Fig. 3. The posterior localization of D-EndoB depends on cellular polarity and Oskar in *Drosophila* oocytes. (A-C) Double labeling of Gurken (red) and D-EndoB (green) in the wild type (A) and *gurken* null mutant (B). Wild-type ovary treated with colcemid (100 µg/ml) for 12 hours was labeled with Gurken (red) and D-EndoB (green) antibodies (C). (D-L) Distribution of Oskar (D), Vasa (G), and D-EndoB (J) could be detected in the oocyte posterior in wild type. In the *D-endoB*^{54} homozygous oocyte, Oskar (F) and Vasa (I) remained enriched at the oocyte posterior pole, compared with *osk*^{54}*/Df(3R)p*^{XT103} (E) and *vasa*^{PH165} (H) mutant oocytes. The localization of D-EndoB was affected in the absence of Oskar (L; *n*=1/18), but only slightly affected in the absence of Vasa (K; *n*=9/10).

D-EndoB is a membrane-associated protein and is involved in endocytosis

Long Oskar has been demonstrated to affect yolk protein endocytosis (Vanzo et al., 2007), and the yolk content is significantly altered in the *D-endoB* mutant oocyte (Fig. 2D). Given that Long Oskar determines the localization of D-EndoB, we further investigated whether D-EndoB is involved in yolk protein endocytosis by examining the ultrastructural localization of D-EndoB. Using electron microscopy, numerous tubulovesicular structures were detected in the oocyte posterior, and the D-EndoB immunogold was mainly localized to these structures (Fig. 5A,D,G). The specificity of this labeling was verified by the absence of immunogold labeling in *D-endoB* mutant egg chambers (Fig. 5B,E). Furthermore, upon observing ectopic expression of *D-endoB* driven by *nanos-Gal4* in the oocyte, a significant increase of labeling signal appeared on the tubulovesicular structures compared with a low non-specific signal increase in mitochondria (Fig. 5C,F).

Similarly, we also observed that the yolk receptor Yolkless was enriched at the tubulovesicular membrane in the wild-type and *D-endoB*^{54} mutant oocytes (Fig. 6Aa,Ab). This is consistent with a previous report (Vanzo et al., 2007) showing that an enormous amount of endocytosis and yolk processing is taking place in the

Development (2014) doi:10.1242/dev.097022

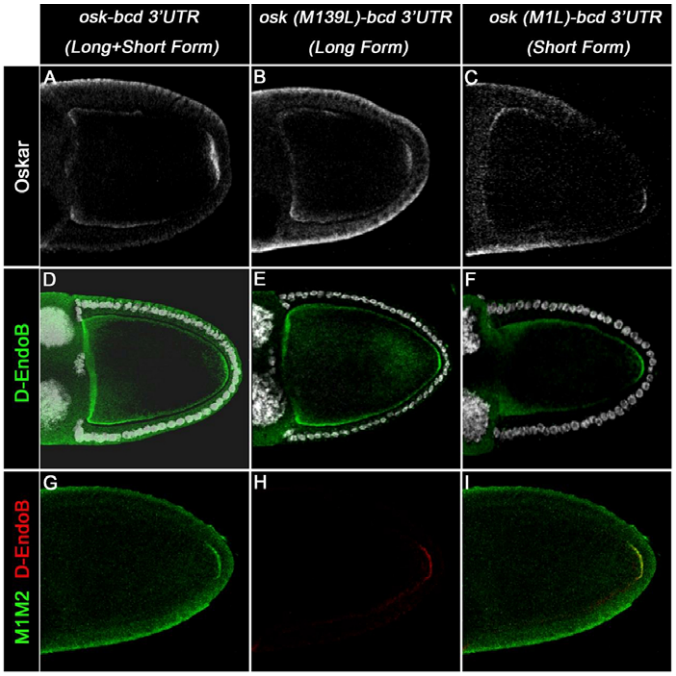

Fig. 4. Ectopically expressing Oskar recruits D-EndoB to the anterior pole of the oocyte. (A-F) Ectopic expression of Oskar at the anterior of the oocyte by *nanos-GAL4*. (A-C) Oskar was localized at the anterior pole under the expression of three transgenes. (D-F) Ectopic D-EndoB could be detected under the expression of both Oskar isoforms (*n*=27) (D) and Long Oskar alone (*n*=11) (E); it could not, however, be detected under the expression of Short Oskar (*n*=20) (F). (G-I) Colocalization of Long Oskar (G, green) and D-EndoB (H, red) at the oocyte posterior.

posterior area near the cortical membrane of the oocyte. The double immunogold staining data showed that D-EndoB and Yolkless were partially colocalized (Fig. 6Ac-Ae, arrowheads), suggesting that D-EndoB is associated with the membrane structures involved in Yolkless-mediated endocytosis. To dissect whether D-EndoB affects Yolkless trafficking, we analyzed the tubulovesicular membrane density and its Yolkless concentration in the *D-endoB* mutant. The tubulovesicular membrane density and yolkless distribution was not altered in the mutant (Fig. 6Aa,Ab; supplementary material Fig. S6A,B). However, a dilation of the tubulovesicular structure in *D-endoB* mutant was noticed (Fig. 6Aa,Ab), and this alteration was statistically significant (supplementary material Fig. S6C). These results are consistent with the role of Endophilin B family proteins in membrane dynamics. Thus, D-EndoB might regulate yolk uptake by controlling membrane dynamics.

D-EndoB is colocalized with Long Oskar on the same tubulovesicular structure

D-EndoB and Long Oskar were found to colocalize in the posterior pole of the oocyte cortex by immunostaining analysis (Fig. 4G). Long Oskar is specifically associated with the endocytic membrane at the posterior pole (Fig. 6Bb) (Vanzo et al., 2007). We found that D-EndoB was partially colocalized with Long Oskar at the same tubulovesicular structures (Fig. 6Bb-Be, arrowheads), but no direct interaction between these two proteins was detected by yeast two hybrid assay (supplementary material Fig. S7A,C). In the absence of D-EndoB, Long Oskar was still detected in the membrane-associated vesicles (Fig. 6Ba), indicating that the localization of Long Oskar is not affected by D-EndoB, which is consistent with the immunofluorescence staining results (Fig. 3F). These results suggest that D-EndoB might function downstream of Long Oskar. Vasa is a downstream factor of the Oskar-regulated pathway, and is also frequently used as a germ cell-specific marker. Vasa was detected abundantly in polar granules (Fig. 6Cb), but D-EndoB was merely localized in these regions in immunoelectron microscopy data (Fig. 6Cc-Ce). The different localization of D-EndoB and Vasa supports the conclusion that these two molecules have different functions. Also, loss of D-EndoB did not affect the Vasa localization (Fig. 3K; Fig. 6Ca). Taken together, we conclude that even though Vasa and D-EndoB both function downstream of Oskar, D-EndoB regulates the yolk protein endocytosis, whereas Vasa participates in pole plasm assembly.

D-EndoB regulates endocytosis activity in the oocyte

Our data presented above is the first study suggesting a role for D-EndoB in endocytosis. However, Endophilin B has been reported to be involved in regulating the membrane curvature during the various membrane dynamic processes (Farsad et al., 2001; Karbowski et al., 2004; Takahashi et al., 2011; Yang et al., 2006). To analyze the possible endocytic role of D-EndoB, we performed the FM4-64 dye uptake assay for visualizing endocytosis in the oocyte. The signal of the fluorescent dye was observed all over the oocyte cortex and was especially enriched at the posterior in the wild-type and $D\text{-}endoB^{54}$ heterozygous oocyte (Fig. 7A,B). However, in the absence of D-EndoB in the oocyte, the enrichment of the signal was decreased (Fig. 7C). The signal was recovered by expressing the $D\text{-}EndoB^{FL}$ transgene (Fig. 7D). These results indicate that the D-EndoB functions in regulating endocytosis in the oocyte. Moreover, we found that D-EndoB was colocalized with Rab5 and Rab7 (supplementary material Fig. S8). To dissect further in which endocytic steps D-EndoB is involved, we performed genetic interaction between D-EndoB and endocytic components by FM4-64 incorporation assay. Although Rbsn5, the Rab5 effector protein, did not interact with D-EndoB genetically (Table 1) (Morrison et al., 2008), D-EndoB displayed significant genetic interaction with the Sec5-Sec6 complex (Fig. 7E-H; Table 1), which regulates the endocytic recycling of Yolkless (Langevin et al., 2005; Sommer et al., 2005). In addition, D-EndoB overexpression suppressed the dominant effect of the *Rab7* mutant in reducing the posterior endocytic activity (Fig. 7I-L; Table 1). These results suggest that D-EndoB may function at multiple steps during endocytosis. However, whether the effect of D-EndoB is direct or indirect remains to be determined.

The N-BAR domain, but not the SH3 domain, contributes to the function of D-EndoB in yolk endocytosis

Drosophila and mammalian endophilin A have been demonstrated to function in clathrin-mediated endocytosis by interacting with dynamin through its SH3 domain (Ringstad et al., 1997; Verstreken et al., 2002). To investigate further whether D-EndoB participates in endocytosis as does Endophilin A, we first tested the interaction with Shibire, which is the *Drosophila* dynamin, by performing a yeast-two hybrid analysis. However, no interaction was observed (supplementary material Fig. S7B,C). Indeed, $D\text{-}EndoB^{\Delta SH3}$, a SH3 deleted mutant (Fig. 8A), expressed in a *D-endoB* mutant background, showed a normal localization and rescued the fecundity, similar to $D\text{-}EndoB^{FL}$ (Fig. 8B,C). These data demonstrate that the SH3 domain of D-EndoB is dispensable for its localization and function in egg production. Next, the N-BAR domain of D-EndoB was examined. Although the $D\text{-}EndoB^{\Delta H0}$ that contained the truncated N-BAR domain (Fig. 8A) showed normal localization (Fig. 8B), its ability to rescue the fecundity was not as strong as that of $D\text{-}EndoB^{FL}$ or $D\text{-}EndoB^{\Delta SH3}$ even at similar expression levels

Development (2014) doi:10.1242/dev.097022

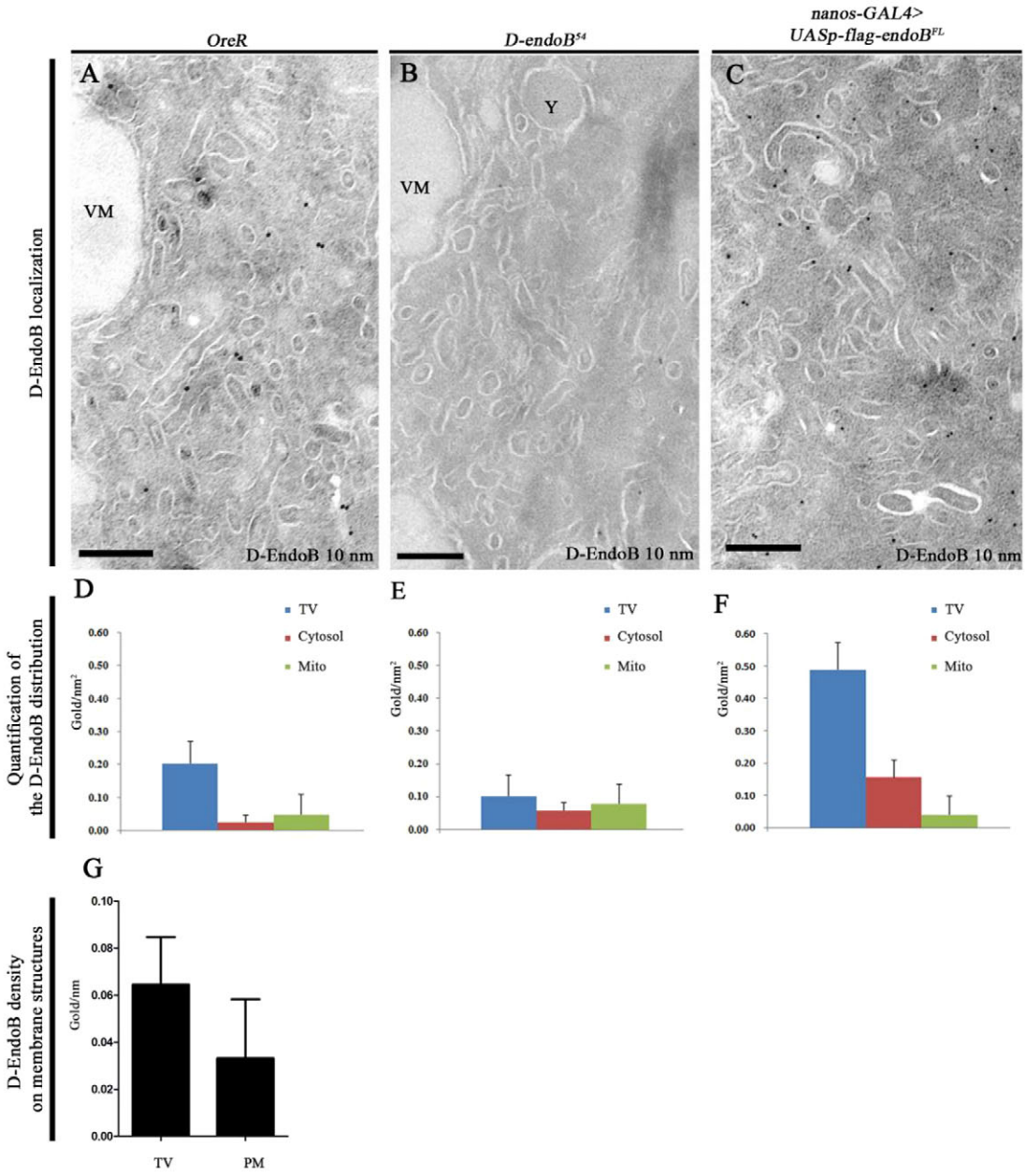

Fig. 5. Ultrastructural localization of D-EndoB. (A-C) Ultrathin cryosections from the mid-planes of late stage 9 oocytes of wild type (A), *D-endoB*^{54} (B) and *nanos-GAL4>UASp-flag-endoB* (C) were immunolabeled for D-EndoB. Images were taken at the posterior pole of the oocytes. Scale bars: 200 nm. (D-F) Semi-quantification of immunogold signals over respective area. Note that in wild type (D), D-EndoB was mainly localized to tubulovesicular structures, whereas only background labeling was observed in *D-endoB*^{54} (E). Overexpression of exogenous D-EndoB resulted in an increased labeling signal primarily at the tubulovesicular compartment (F). Total areas examined were 8.19 μm^2 (OreR, *n*=5), 7.3 μm^2 (*D-endoB*^{54}, *n*=4) and 4.9 μm^2 (D-EndoB^{FL}, *n*=6). (G) Apart from tubulovesicular membranes, D-EndoB was also found at the plasma membrane. Total contour length examined was 36.2 μm (*n*=4). Mito, mitochondria; PM, plasma membrane; TV, tubulovesicular structures.

(Fig. 8C; supplementary material Fig. S3A). These data suggest that the full function of D-EndoB requires the intact N-BAR domain, but not the SH3 domain.

To reveal further effects of D-EndoB overexpression in the ovary, the development of egg chambers was examined. The newly eclosed females were collected and fed with yeast powder at 25°C for 36 hours (He et al., 2011), and then the composition of each ovariole with different stages of developing egg chambers was analyzed. Ovarioles from OreR females were classified in the following two groups: one group contained at least one middle stage egg chamber (vitellogenic stage 8-10) and one late stage egg chamber (Fig. 8D, red bar, 56.3%), and the other group contained only one middle stage egg chamber (Fig. 8D, blue bar, 42.3%). In the *D-endoB* null ovariole, ~14% of the ovarioles contained only one late and some early stage egg chambers, but lacked middle stage egg chambers (Fig. 8D, green bar, 14.5%). Although ectopically expressing *D-endoB*^{FL} and *D-endoB*$^{\Delta SH3}$ under *D-endoB* null background rescued the 15% of ovarioles that lack middle stage egg chambers, *D-endoB*$^{\Delta H0}$ only restored 5% of the ovarioles with this defect (Fig. 8D). Taken together, *D-endoB*^{FL} and *D-endoB*$^{\Delta SH3}$ accelerate the process of vitellogenesis, and this may lead to higher fecundity than that found in wild-type females.

Development (2014) doi:10.1242/dev.097022

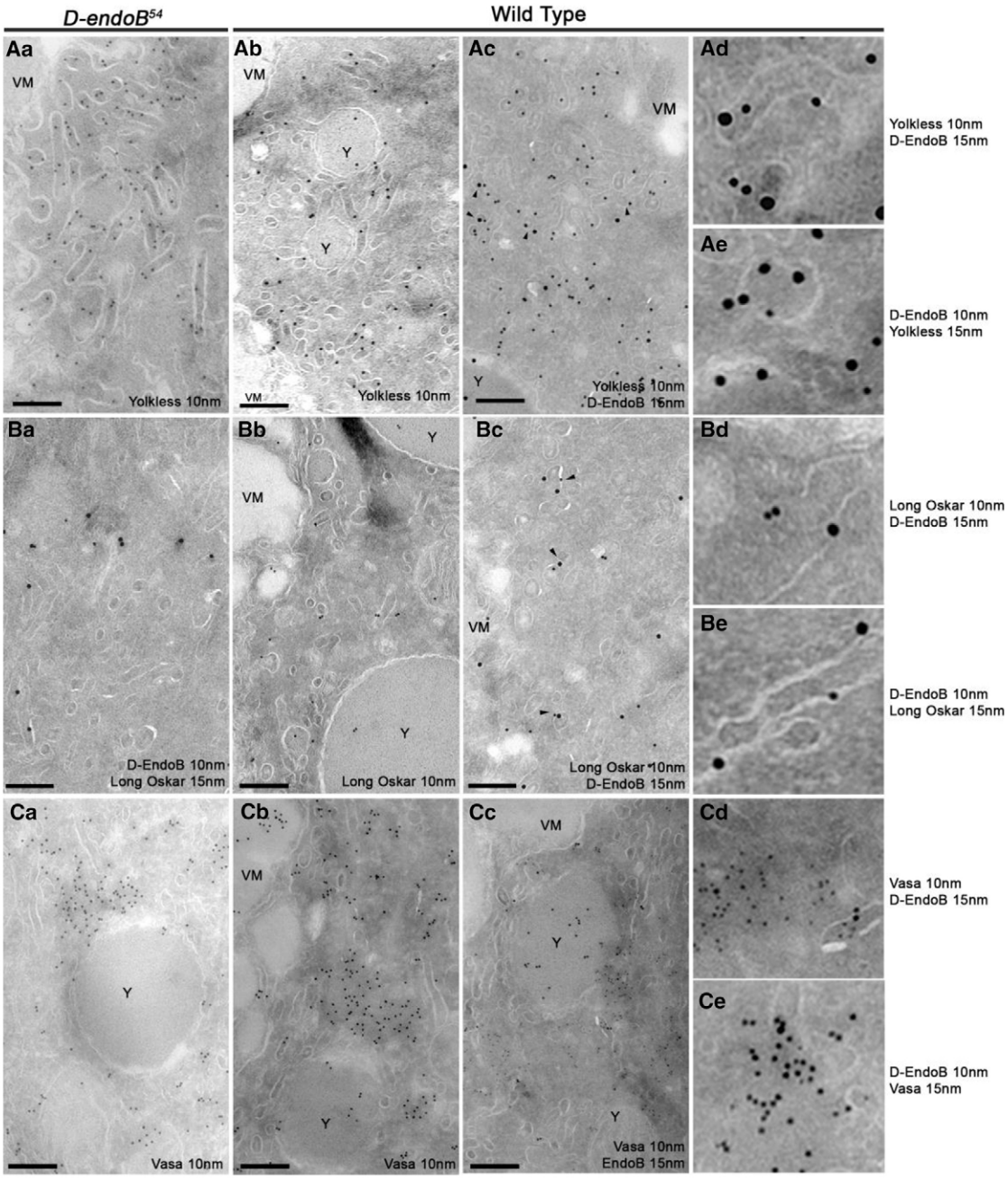

Fig. 6. D-EndoB partially colocalizes with Long Oskar and Yolkless but not Vasa. (Aa-Ce) Micrographs of the posterior pole of immunolabeled late stage 9 oocytes from *D-endoB*^{54} mutant (Aa,Ba,Ca) and wild-type (Ab-Ae, Bb-B3, Cb-Ce) flies. (Aa-Ae) The tubulovesicular membranes were heavily labeled with Yolkless with which D-EndoB was partially colocalized (Ac-Ae, arrowheads in Ac). (Ba-Be) Long Oskar was also localized to the tubulovesicular membranes with which D-endoB was partially colocalized (Bc-Be, arrowheads in Bc). Only background staining of D-EndoB was detected in the *D-endoB*^{54} mutant (Ba). The localization of Vasa (Ca-Ce) to polar granules was not affected by the absence of D-EndoB (Ca). Scale bars: 200 nm. VM, vitelline membrane; Y, yolk granule.

DISCUSSION

In this study, we provide evidence that Endophilin B is involved in the endocytic process of yolk uptake during *Drosophila* oogenesis. Although the receptor for yolk protein endocytosis (Yolkless) is evenly distributed in the ooplasm, a posterior locally active endocytic process has recently been revealed (Vanzo et al., 2007). The Oskar asymmetric posterior localization depends on anteroposterior polarity established by Gurken signaling, and Long Oskar recruits the endocytic component to maintain polarity for pole plasm anchorage and active endocytosis (Tanaka and Nakamura, 2008). D-EndoB is recruited by Long Oskar but is not involved in polarity maintenance. Furthermore, Oskar-induced F-actin remodeling is not affected by D-EndoB (data not shown), indicating that D-EndoB functions downstream of F-actin establishment.

Here, we demonstrate that the endocytic machinery in the oocyte is crucial for yolk deposition and vitellogenesis, as in the *D-endoB* mutant, the yolk content and the progress of vitellogenesis are significantly reduced; however, the germline stem cell development, maintenance, and cystoblast differentiation are not influenced (data not shown). Indeed, the expression level of D-EndoB is positively

Development (2014) doi:10.1242/dev.097022

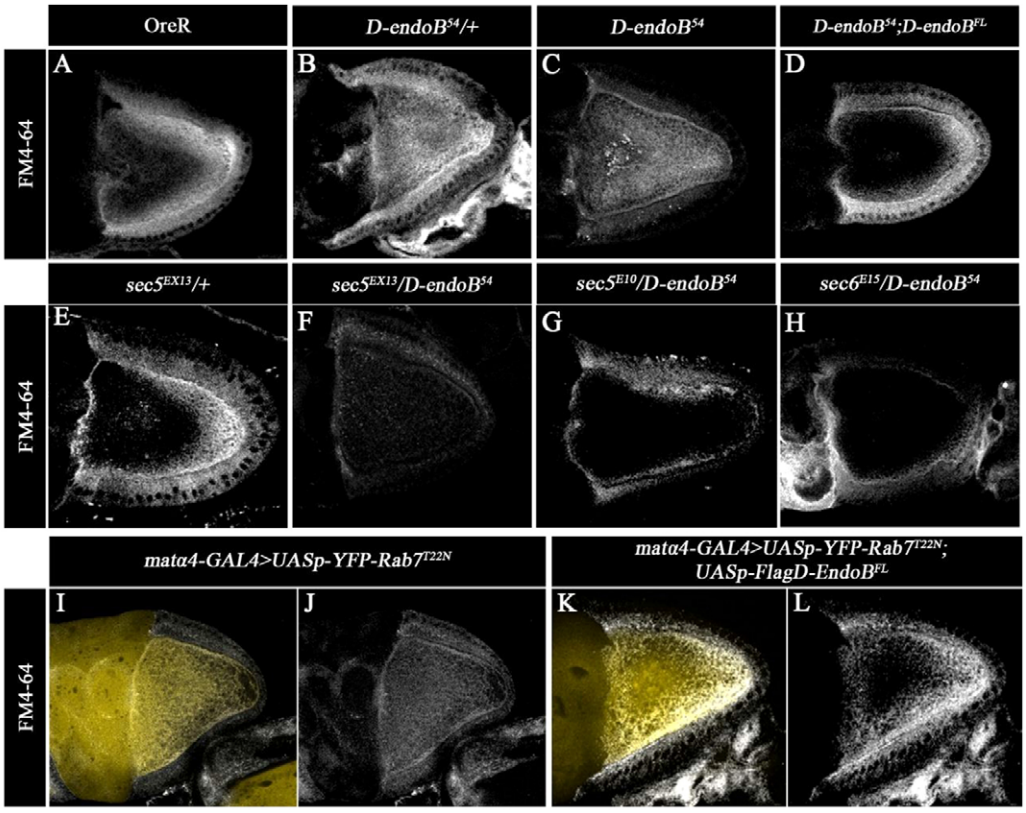

Fig. 7. Endocytic activity within the *Drosophila* oocyte requires D-EndoB. (A-D) Detection of endocytic activity by FM4-64 dye incorporation. High-level signal at the oocyte posterior was detected in wild-type (A; 85.7%, *n*=22), *D-endoB*^{54} heterozygous (B; 81.82%, *n*=22) and D-EndoB-rescued *D-endoB* null (D; 70.5%, *n*=17) oocytes but not in *D-endoB* null oocytes (C; 26.3%, *n*=19). (E-H) In the genetic interaction assay, high-level of signal could also be detected in *sec5*^{EX13} heterozygous (E), but not in transheterozygote of *D-endoB*^{54} and *sec5*^{EX13} (D), *sec5*^{E10} (E) or *sce6*^{E15} (F) mutant alleles. (I-L) The same assay was performed in oocytes expressing the dominant-negative Rab7-YFP alone (I,J) or with the co-expression of D-EndoB^{FL} transgene (K,L). Note that the quantification of the genetic experiment is summarized in Table 1.

correlated with egg production; for example, a high level of D-EndoB resulted in a 30% increase in fecundity (Fig. 8C). Our results suggest that the dosage effect of D-EndoB could result from the promotion of vitellogenesis progression (Fig. 8D). Given that D-EndoB was ectopically expressed in the oocyte, it seems that the yolk content of a more mature egg chamber may send a signal to a younger egg chamber to promote the entry into vitellogenesis. To our surprise, we found that an endocytic component can participate in this checkpoint during oogenesis. Taken together, D-EndoB acts downstream of Oskar to mediate the asymmetric endocytic activity and facilitates yolk protein deposition into the oocyte, which leads to the acceleration of vitellogenesis and thus improves fecundity.

In mammalian cell culture, the N-BAR domain of endophilin B1 alone is not sufficient to promote autophagosome formation, suggesting that the SH3 domain is crucial for participating in a specific cellular process (Takahashi et al., 2011). We discovered that D-EndoB does not interact with Dynamin (supplementary material Fig. S7B), suggesting that it does not function at the fission reaction. Interestingly, Milosevic and colleagues also found that endophilin A is important for uncoating instead of fission reaction (Milosevic et al., 2011). Similarly, endophilin A lacking the SH3 is still functional in the *Caenorhabditis elegans* axon (Bai et al., 2010). Moreover, SH3 domain-deleted D-EndoB$^{\Delta SH3}$ still promotes enriched localization at the posterior pole of the oocyte and displays full ability in rescuing fecundity defect in *D-endoB*^{54} null mutant females (Fig. 8C). Thus, the protein-protein interaction function of the SH3 domain is not required for the function and localization of D-EndoB in the endocytic process during yolk

Table 1. Genetic interactions between D-EndoB and endocytic components

A. Genetic interaction assay between D-EndoB and Rbsn-5, Sec5 or Sec6

	rbsn-5^{C241}/+	rbsn-5^{C241}/ D-endoB^{54}	sec5^{E13}/+	sec5^{E13}/ D-endoB^{54}	sec5^{E10}/+	sec5^{E10}/ D-endoB^{54}	sec6^{Ex15}/+	sec6^{Ex15}/ D-endoB^{54}	D-endoB^{54}/+
Percentage of oocytes with endocytic activity*	70.6	88.9	73.9	24	87.5	26.1	78.6	22.7	81.8
Total	17	18	23	25	24	23	14	22	22

B. Co-expression of D-EndoB with dominant-negative Rab7 or Rab11 in the germline cell

	matα4-GAL4>UASp-YFP-Rab7^{T22N}	matα4-GAL4>UASp-YFP-Rab7^{T22N};UASp-Flag-D-EndoB^{FL}	nanos-GAL4>UASp-YFP-Rab11^{S25N}	nanos-GAL4>UASp-YFP-Rab11^{S25N};UASp-Flag-D-EndoB^{FL}
Percentage of oocytes with endocytic activity*	23.5	84.6	77.8	N.D.‡
Total	17	26	9	N.D.‡

*Determined by FM4-64 dye incorporation.
‡No middle stage egg chambers were observed.
N.D., not done.
Total denotes number of oocytes examined.

Development (2014) doi:10.1242/dev.097022

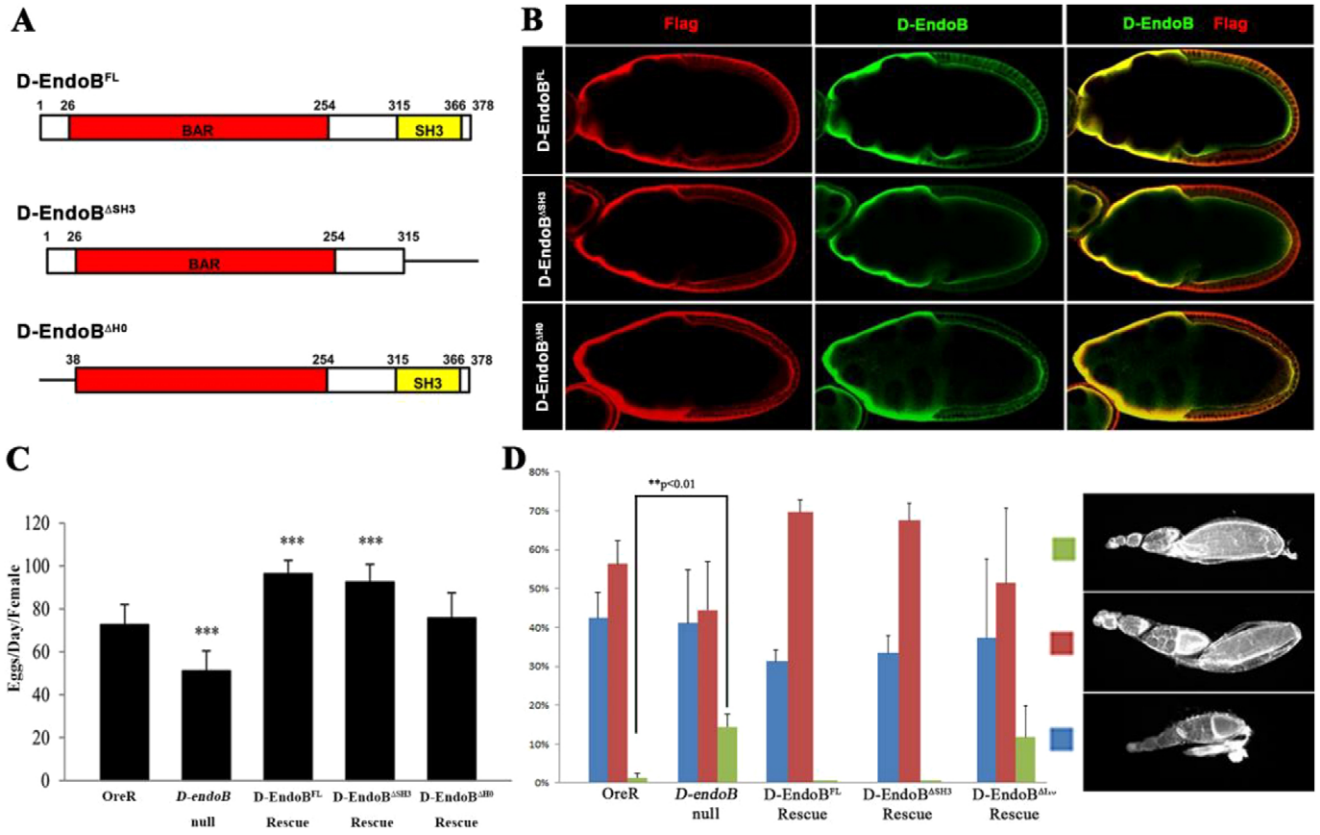

Fig. 8. The function of D-EndoB requires the N-BAR domain. (A) Illustration of each *D-endoB* transgene. The full length *D-endoB*, *D-endoB*^{FL}, contains intact N-BAR (amino acids 26-254) and SH3 (amino acids 315-366) domains. The *D-endoB*$^{\Delta SH3}$ lacks the 315-378 amino acid fragment that encodes the SH3 domain. In the N-BAR domain truncated mutant, *D-endoB*$^{\Delta H0}$, the first 38 amino acids were deleted. (B) Immunostaining of the different *D-endoB* transgenes, which were fused with a Flag tag under *D-endoB* mutant background. Stage 9 egg chambers expressing *D-endoB*^{FL} (*n*=20/24), *D-endoB*$^{\Delta SH3}$ (*n*=22/28) and *D-endoB*$^{\Delta H0}$ (*n*=19/24) were immunostained with anti-Flag (red) or anti-D-EndoB (green) antibodies. Merged images show an overlap of Flag and D-EndoB staining patterns in the oocyte. (C) Egg production of OreR females (mean ± s.d.; *n*=20), *D-endoB*^{54}*/Df(2R)BSC26* females (mean ± s.d.; *n*=19) and each rescued female: *D-endoB*^{FL} (mean ± s.d.; *n*=16), *D-endoB*$^{\Delta SH3}$ (mean ± s.d.; *n*=13) and *D-endoB*$^{\Delta H0}$ (*n*=21). ***P<0.001. (D) Dissection of the oogenesis stage of each ovariole. Ovarioles of indicated *D-endoB* transgene expressed under D-endoB null background were counterstained with phalloidin. OreR (*n*=222 ovarioles), *D-endoB*^{54}*/Df(2R)BSC26* (*n*=353 ovarioles), *D-endoB*^{FL} (*n*=291 ovarioles), *D-endoB*$^{\Delta SH3}$ (*n*=278 ovarioles) and *D-endoB*$^{\Delta H0}$ (*n*=275 ovarioles). **P<0.01.

uptake in *Drosophila* ovaries, suggesting that the N-BAR domain may be sufficient for the function of D-EndoB in yolk protein endocytosis.

N-BAR domain contains two N-terminal amphipathic helixes, H0 and H1I, and a crescent-shaped main body to perform binding and to tubulate the liposome membrane. The H0 region contributes to the membrane binding and H1I subsequently inserts into the membrane, their shape allowing them to associate with curved membranes (Peter et al., 2004). When we express the *D-endoB*$^{\Delta H0}$ transgene, its ability to rescue the fecundity phenotype is reduced compared with a *D-endoB*^{FL} transgene of similar expression level (Fig. 8C). This indicates that H0 is required for the full function of D-EndoB. Although previous reports show that H0 is important in N-BAR domain function during autophagosome formation or liposome tubulation, it is still possible that the H1I of the BAR domain is able to sense the already curved membrane (Gallop et al., 2006; McMahon and Gallop, 2005). Furthermore, we did not detect a significant reduction of endocytic structures or yolkless distribution in the *D-enodB*^{54} homozygous mutant oocyte (Fig. 5B; Fig. 6Aa; supplementary material Fig. S6B), suggesting that the D-EndoB may function in associating with the bent oocyte membrane to enhance the yolk protein endocytosis but it plays a minor role in directly inducing the endocytic structure.

In this study, we demonstrate that D-EndoB responds to Oskar-regulated endocytosis to regulate the yolk content (Vanzo et al., 2007). *D-endoB* genetically interacts with *rab7* and the *sec5/6* complex, suggesting that it may be involved in multiple steps of endocytic process (Fig. 7). Here, we propose a model in which the Oskar protein regulates an endocytic pathway for remodeling the cytoskeleton, which establishes an environment filled with active endocytic structures in the oocyte posterior. Once a curved membrane is generated, D-EndoB can sense and bind to this membrane to facilitate the further deformation of these membrane structures, which then enhances the endocytosis of the yolk protein and thus leads to accelerated egg maturation. Indeed, a dilation of tubulovesicular structure was observed in *D-endoB* mutant oocyte cortex (Fig. 6Aa,Ab; supplementary material Fig. S6C), indicating that the membrane dynamics might slow down in the absence of D-EndoB. Therefore, D-EndoB participates in the polarized endocytic activity of yolk uptake by Oskar in the oocyte.

MATERIALS AND METHODS

Fly stocks

OreR (*Oregon-R*) was used as the wild-type control. *D-endoB*^{54} is a *D-endoB* null mutant line generated in this study. *Df(2R)BSC26* (Bloomington Stock Center) uncovers the *D-endoB* gene. The following mutant stocks

Development (2014) doi:10.1242/dev.097022

were used: *vasa*^{PH165} (Styhler et al., 1998), *osk*^{54}/*Df(3R)p*^{XT103} (Kim-Ha et al., 1991), *grk*^{2B6} (Neuman-Silberberg and Schüpbach, 1996), *grk*^{HF} (Schüpbach, 1987), *sec5*^{E10} and *sec5*^{E13} (Murthy et al., 2003), *sec6*^{Ex15} (Murthy et al., 2005) and *rbsn5*^{C241} (Tanaka and Nakamura, 2008). The following transgenes were driven by *nanos-GAL4* or *matα-GAL4* to be expressed ectopically in the oocyte: *osk-bcd 3′UTR*, *osk(M139L)-bcd 3′UTR*, *osk(M1L)-bcd 3′UTR* (Tanaka and Nakamura, 2008), *UASp-YFP-Rab5*, *UASp-YFP-Rab11*, *UASp-YFP-Rab7*^{T22N} and *UASp-YFP-Rab11*^{S25N} (Bloomington Stock Center).

D-endoB transgene

A *Bam*HI/*Xba*I fragment (nt 1-1137) of full-length *D-endoB* cDNA was PCR amplified by primers (5′-GGGGATCCTGAACCGTCAGA-ATTGATCTAC-3′ and 5′GCTCTAGATTAGAGGGTGACATCGTG-CTCTTC-3′), and subcloned into a Flag-tagged fusion UASp vector for generation of the *D-endoB*^{FL} transgene. To generate *D-endoB*$^{\Delta SH3}$ and *D-endoB*$^{\Delta H0}$ mutant transgenes, a *Bam*HI/*Xba*I fragment excluding the D-EndoB SH3 domain (nt 1-938) was amplified by primers (5′-GGGGATCCTGAACCGTCAGAATTGATCTAC-3′ and 5′-ATTTCT-AGATTAGTGAACCGTCAGAATTGATCTACC-3′) and a *Eco*RI/*BamHI* fragment lacking the H0 region of D-EndoB N-BAR domain (nt 118-1137) was amplified by primers (5′-GGGAATTCTACGACTT-GCACTTCCAGAATCTCGCC-3′ and 5′-GGGGATCCTTAGAGG-GTGACATCGTGCTCTTCGTC-3′). The amplified fragments were then subcloned into a Flag-tagged fusion UASp vector.

Antibody generation

A full-length *cg9834* open reading frame (ORF) was cloned into *pET32a* vector to express a 6xHis-tagged D-EndoB fusion protein and was then purified by Ni-NTA beads (Qiagen). The obtained polyclonal rabbit antibody against this fusion protein was affinity purified and pre-absorbed, and was used for immunostaining (1:100) and western blotting (1:500). A similar strategy was used to generate guinea pig anti-M1M2 and rabbit anti-Yolkless antibodies. PCR amplification of a long *oskar*-specific 413-bp *Nco*I/*Bam*HI fragment was cloned into *pET32a* vector and the fusion protein was purified for raising guinea pig polyclonal antibodies. *pET32b-yolkless* contained a 666-bp *Bam*HI/*Sal*I of a *yl* cDNA fragment which encodes a 222-amino acid polypeptide with three of the C-terminal repeats (amino acids 752-973).

Immunofluorescence staining

Ovaries from 2- to 3-day-old females were fixed in 4% paraformaldehyde for 20 minutes. For embryo staining, embryos were fixed in 9% formaldehyde. Fixed embryos were then devitellinized by methanol. Rehydrated embryos were blocked in 2% bovine serum albumin. Primary antibodies were applied overnight in blocking solution: rabbit anti-D-EndoB (1:100; lab stocks), guinea pig anti-M1M2 (1:500; lab stocks), mouse anti-Gurken [1:100; Developmental Studies Hybridoma Bank (DSHB)], rabbit anti-Oskar (1:1000; Ephrussi Laboratories), rat anti-Vasa (1:50; DSHB) and mouse anti-Flag (1:50; Sigma). Samples were then labeled with secondary antibodies (1:500; Invitrogen). Samples were observed by a Zeiss confocal microscope.

FM4-64 dye uptake assay

FM4-64 dye uptake assays were previously described (Sommer et al., 2005). Briefly, ovaries were dissected in *Drosophila* Schneider's medium (Gibco) containing 10 μM FM 4-64 dye (Invitrogen). After incubating for 30 minutes, ovaries were back-extracted for 15 minutes with PBS at 4°C and directly observed with a Zeiss confocal microscope.

Fecundity and hatching assay

Newly eclosed flies (2-3 days) were collected and each female was coupled with one male fly on a juice plate with wet yeast. After two days, the eggs laid by each female were counted every day for four days. To calculate the percentage of hatching, eggs laid on grape juice-agar plates were incubated at 25°C over 24 hours and hatched embryos were counted.

Yeast two-hybrid assay

The full-length *D-endoB*, *oskar* and *Drosophila dynamin* (*shibire*) were amplified from a *Drosophila* ovarian cDNA library by PCR. Amplified *D-endoB* was cloned into the *pGBKT7* vector (Clontech) to fuse with GAL4 binding domain. *oskar* and *shibire* was constructed into *pGADT7* to fuse with the activating domain of GAL4 protein. *pGBKT7-D-endoB* carrying *TRP1* gene was co-transformed into yeast YH109 strain (Clontech) with *pGADT7-shibire* or *pGADT7-oskar* carrying the *LEU2* gene following double selection on leucine-tryptophan drop-out plates.

In situ hybridization

The D-EndoB sense and anti-sense probe were amplified from full-length *cg9834* ORF by T3 RNA polymerase (Roche) and T7 RNA polymerase (Roche). The RNA hybridization procedure was performed as previously described (Tautz and Pfeifle, 1989).

Electron microscopy

Sample preparation

Egg chambers were processed for ultracryomicrotomy as described previously (Chang et al., 2008). To obtain mid-horizontal sections, serial semi-thin sections of 1 μm thickness were first cut at –70°C, and examined with a light microscope after staining with 0.1% Toluidine Blue. When follicle cells appeared single-layered, indicating that the mid-plane had been reached, the cutting temperature was lowered to –100°C and section thickness switched to 55 nm. Sections were contrast-stained with uranyl acetate for morphometric analysis or immunolabeled for localization studies. Primary antibodies were as follows: rabbit anti-Yolkless, anti-D-EndoB, anti-M1M2 (all generated in house) and rat anti-Vasa (DSHB). Rabbit antibodies were recognized by protein-A-gold (CMC-UMC, Utrecht). Rat antibodies were detected by a rabbit anti-rat IgG (Jackson ImmunoResearch) followed by the protein-A-gold. Double labeling procedures were performed sequentially as described (Slot et al., 1991).

Quantitative EM

Yolk volume density (Vv)

Equatorial sections of late stage 9 egg chambers were used to compare the yolk volume density in the cortical versus central ooplasm. The cortical area was arbitrarily defined as the oocyte region that spans 10 μm in depth from the oolemma; the rest of the ooplasm was considered central. Six pictures of non-overlapping fields were randomly taken from each egg chamber of respective genotypes: three micrographs from the cortical and three from the central ooplasm. The yolk granules were defined as dense and round objects. Yolk volume density (Vv) relative to the ooplasm was estimated by the point counting method for every picture taken and analyzed (Weibel, 1969).

D-EndoB immunogold distribution

The posterior cytoplasm beneath 1 μm of plasma membrane was analyzed. Labeling density over respective structures was expressed as gold particles per area (point counts). D-EndoB concentration over the tubulovesicular membrane and plasma membrane was expressed as gold particles per contour length (intersection counts) (Griffiths et al., 1993).

Surface density (Sv) of tubulovesicular structure

Tubulovesicular structures within the posterior cytoplasm beneath 1 μm of plasma membrane were quantified for membrane and surface density (Sv, expressed as ratio of intersection versus point count), as well as Yolkless concentration (gold/length).

Acknowledgements

We thank Drs T. B. Chou, M. D. Lin, A. Ephrussi and T. L. Schwarz, Fly Core Taiwan, Bloomington *Drosophila* Stock Center and the Developmental Studies Hybridoma Bank for fly stocks and reagents. We thank Drs Trudi Schupbach, Scott C. Schuyler, Chien-Kuo Lee and S. Y. Yang for their comments and the members of Pai lab for the valuable discussions.

Competing interests

The authors declare no competing financial interests.

Author contributions

L.-M.P. conceived the project. Y.-C.T. performed the cloning, WB and IF experiments. W.C. performed EM experiments and analyzed the data with W.L. Antibodies were generated by Y.-C.T., W.C. and W.-H.L. Y.-W.C. discovered the D-EndoB localization. P.-Y.W. performed the Y2H experiment. Y.-C.L. established the *D-endoB*^{54} mutant. T.T. and A.N. edited the paper. L.-M.P., W.L. and Y.-C.T. wrote the paper.

Funding

This work was supported by grants from the National Science Council of Republic of China [NSC100-2311-B-182-001-MY3 to L.P.]; the Chang Gung Memorial Hospital [CMRPD180111-3 to L.P.; CMRPD100031 and CMRPD1B0281 to W.L.]; and the Ministry of Education, Taiwan, ROC [EMRPD1C0041 to L.P.].

Supplementary material

Supplementary material available online at
http://dev.biologists.org/lookup/suppl/doi:10.1242/dev.097022/-/DC1

References

Bai, J., Hu, Z., Dittman, J. S., Pym, E. C. and Kaplan, J. M. (2010). Endophilin functions as a membrane-bending molecule and is delivered to endocytic zones by exocytosis. *Cell* **143**, 430-441.

Bownes, M., Scott, A. and Shirras, A. (1988). Dietary components modulate yolk protein gene transcription in Drosophila melanogaster. *Development* **103**, 119-128.

Breitwieser, W., Markussen, F. H., Horstmann, H. and Ephrussi, A. (1996). Oskar protein interaction with Vasa represents an essential step in polar granule assembly. *Genes Dev.* **10**, 2179-2188.

Brennan, M. D., Weiner, A. J., Goralski, T. J. and Mahowald, A. P. (1982). The follicle cells are a major site of vitellogenin synthesis in Drosophila melanogaster. *Dev. Biol.* **89**, 225-236.

Chang, W. L., Liou, W., Pen, H. C., Chou, H. Y., Chang, Y. W., Li, W. H., Chiang, W. and Pai, L. M. (2008). The gradient of Gurken, a long-range morphogen, is directly regulated by Cbl-mediated endocytosis. *Development* **135**, 1923-1933.

Compagnon, J., Gervais, L., Roman, M. S., Chamot-Boeuf, S. and Guichet, A. (2009). Interplay between Rab5 and PtdIns(4,5)P2 controls early endocytosis in the Drosophila germline. *J. Cell Sci.* **122**, 25-35.

Dawson, J. C., Legg, J. A. and Machesky, L. M. (2006). Bar domain proteins: a role in tubulation, scission and actin assembly in clathrin-mediated endocytosis. *Trends Cell Biol.* **16**, 493-498.

DiMario, P. J. and Mahowald, A. P. (1987). Female sterile (1) yolkless: a recessive female sterile mutation in Drosophila melanogaster with depressed numbers of coated pits and coated vesicles within the developing oocytes. *J. Cell Biol.* **105**, 199-206.

Drummond-Barbosa, D. and Spradling, A. C. (2001). Stem cells and their progeny respond to nutritional changes during Drosophila oogenesis. *Dev. Biol.* **231**, 265-278.

Farsad, K., Ringstad, N., Takei, K., Floyd, S. R., Rose, K. and De Camilli, P. (2001). Generation of high curvature membranes mediated by direct endophilin bilayer interactions. *J. Cell Biol.* **155**, 193-200.

Gallop, J. L., Jao, C. C., Kent, H. M., Butler, P. J., Evans, P. R., Langen, R. and McMahon, H. T. (2006). Mechanism of endophilin N-BAR domain-mediated membrane curvature. *EMBO J.* **25**, 2898-2910.

Griffiths, G., Burke. B. and Lucocq J. (1993). *Fine Structure Immunocytochemistry*. Berlin; New York, NY: Springer-Verlag.

He, L., Wang, X. and Montell, D. J. (2011). Shining light on Drosophila oogenesis: live imaging of egg development. *Curr. Opin. Genet. Dev.* **21**, 612-619.

Karbowski, M., Jeong, S. Y. and Youle, R. J. (2004). Endophilin B1 is required for the maintenance of mitochondrial morphology. *J. Cell Biol.* **166**, 1027-1039.

Kim-Ha, J., Smith, J. L. and Macdonald, P. M. (1991). oskar mRNA is localized to the posterior pole of the Drosophila oocyte. *Cell* **66**, 23-35.

Langevin, J., Morgan, M. J., Sibarita, J. B., Aresta, S., Murthy, M., Schwarz, T., Camonis, J. and Bellaïche, Y. (2005). Drosophila exocyst components Sec5, Sec6, and Sec15 regulate DE-Cadherin trafficking from recycling endosomes to the plasma membrane. *Dev. Cell* **9**, 365-376.

Markussen, F. H., Michon, A. M., Breitwieser, W. and Ephrussi, A. (1995). Translational control of oskar generates short OSK, the isoform that induces pole plasma assembly. *Development* **121**, 3723-3732.

Markussen, F. H., Breitwieser, W. and Ephrussi, A. (1997). Efficient translation and phosphorylation of Oskar require Oskar protein and the RNA helicase Vasa. *Cold Spring Harb. Symp. Quant. Biol.* **62**, 13-17.

Masuda, M., Takeda, S., Sone, M., Ohki, T., Mori, H., Kamioka, Y. and Mochizuki, N. (2006). Endophilin BAR domain drives membrane curvature by two newly identified structure-based mechanisms. *EMBO J.* **25**, 2889-2897.

McMahon, H. T. and Gallop, J. L. (2005). Membrane curvature and mechanisms of dynamic cell membrane remodelling. *Nature* **438**, 590-596.

Micheva, K. D., Ramjaun, A. R., Kay, B. K. and McPherson, P. S. (1997). SH3 domain-dependent interactions of endophilin with amphiphysin. *FEBS Lett.* **414**, 308-312.

Milosevic, I., Giovedi, S., Lou, X., Raimondi, A., Collesi, C., Shen, H., Paradise, S., O'Toole, E., Ferguson, S., Cremona, O. et al. (2011). Recruitment of endophilin to clathrin-coated pit necks is required for efficient vesicle uncoating after fission. *Neuron* **72**, 587-601.

Morrison, H. A., Dionne, H., Rusten, T. E., Brech, A., Fisher, W. W., Pfeiffer, B. D., Celniker, S. E., Stenmark, H. and Bilder, D. (2008). Regulation of early endosomal entry by the Drosophila tumor suppressors Rabenosyn and Vps45. *Mol. Biol. Cell* **19**, 4167-4176.

Murthy, M., Garza, D., Scheller, R. H. and Schwarz, T. L. (2003). Mutations in the exocyst component Sec5 disrupt neuronal membrane traffic, but neurotransmitter release persists. *Neuron* **37**, 433-447.

Murthy, M., Ranjan, R., Denef, N., Higashi, M. E., Schupbach, T. and Schwarz, T. L. (2005). Sec6 mutations and the Drosophila exocyst complex. *J. Cell Sci.* **118**, 1139-1150.

Neuman-Silberberg, F. S. and Schüpbach, T. (1996). The Drosophila TGF-alpha-like protein Gurken: expression and cellular localization during Drosophila oogenesis. *Mech. Dev.* **59**, 105-113.

Nilson, L. A. and Schüpbach, T. (1999). EGF receptor signaling in Drosophila oogenesis. *Curr. Top. Dev. Biol.* **44**, 203-243.

Peter, B. J., Kent, H. M., Mills, I. G., Vallis, Y., Butler, P. J., Evans, P. R. and McMahon, H. T. (2004). BAR domains as sensors of membrane curvature: the amphiphysin BAR structure. *Science* **303**, 495-499.

Richard, D. S., Gilbert, M., Crum, B., Hollinshead, D. M., Schelble, S. and Scheswohl, D. (2001). Yolk protein endocytosis by oocytes in Drosophila melanogaster: immunofluorescent localization of clathrin, adaptin and the yolk protein receptor. *J. Insect Physiol.* **47**, 715-723.

Riechmann, V. and Ephrussi, A. (2001). Axis formation during Drosophila oogenesis. *Curr. Opin. Genet. Dev.* **11**, 374-383.

Ringstad, N., Nemoto, Y. and De Camilli, P. (1997). The SH3p4/Sh3p8/SH3p13 protein family: binding partners for synaptojanin and dynamin via a Grb2-like Src homology 3 domain. *Proc. Natl. Acad. Sci. USA* **94**, 8569-8574.

Rørth, P. (1998). Gal4 in the Drosophila female germline. *Mech. Dev.* **78**, 113-118.

Schonbaum, C. P., Lee, S. and Mahowald, A. P. (1995). The Drosophila yolkless gene encodes a vitellogenin receptor belonging to the low density lipoprotein receptor superfamily. *Proc. Natl. Acad. Sci. USA* **92**, 1485-1489.

Schonbaum, C. P., Perrino, J. J. and Mahowald, A. P. (2000). Regulation of the vitellogenin receptor during Drosophila melanogaster oogenesis. *Mol. Biol. Cell* **11**, 511-521.

Schüpbach, T. (1987). Germ line and soma cooperate during oogenesis to establish the dorsoventral pattern of egg shell and embryo in Drosophila melanogaster. *Cell* **49**, 699-707.

Simpson, F., Hussain, N. K., Qualmann, B., Kelly, R. B., Kay, B. K., McPherson, P. S. and Schmid, S. L. (1999). SH3-domain-containing proteins function at distinct steps in clathrin-coated vesicle formation. *Nat. Cell Biol.* **1**, 119-124.

Slot, J. W., Geuze, H. J., Gigengack, S., Lienhard, G. E. and James, D. E. (1991). Immuno-localization of the insulin regulatable glucose transporter in brown adipose tissue of the rat. *J. Cell Biol.* **113**, 123-135.

Sommer, B., Oprins, A., Rabouille, C. and Munro, S. (2005). The exocyst component Sec5 is present on endocytic vesicles in the oocyte of Drosophila melanogaster. *J. Cell Biol.* **169**, 953-963.

Styhler, S., Nakamura, A., Swan, A., Suter, B. and Lasko, P. (1998). vasa is required for GURKEN accumulation in the oocyte, and is involved in oocyte differentiation and germline cyst development. *Development* **125**, 1569-1578.

Sundborger, A., Soderblom, C., Vorontsova, O., Evergren, E., Hinshaw, J. E. and Shupliakov, O. (2011). An endophilin-dynamin complex promotes budding of clathrin-coated vesicles during synaptic vesicle recycling. *J. Cell Sci.* **124**, 133-143.

Takahashi, Y., Coppola, D., Matsushita, N., Cualing, H. D., Sun, M., Sato, Y., Liang, C., Jung, J. U., Cheng, J. Q., Mulé, J. J. et al. (2007). Bif-1 interacts with Beclin 1 through UVRAG and regulates autophagy and tumorigenesis. *Nat. Cell Biol.* **9**, 1142-1151.

Takahashi, Y., Meyerkord, C. L. and Wang, H. G. (2008). BARgaining membranes for autophagosome formation: Regulation of autophagy and tumorigenesis by Bif-1/Endophilin B1. *Autophagy* **4**, 121-124.

Takahashi, Y., Meyerkord, C. L. and Wang, H. G. (2009). Bif-1/endophilin B1: a candidate for crescent driving force in autophagy. *Cell Death Differ.* **16**, 947-955.

Takahashi, Y., Meyerkord, C. L., Hori, T., Runkle, K., Fox, T. E., Kester, M., Loughran, T. P. and Wang, H. G. (2011). Bif-1 regulates Atg9 trafficking by mediating the fission of Golgi membranes during autophagy. *Autophagy* **7**, 61-73.

Tanaka, T. and Nakamura, A. (2008). The endocytic pathway acts downstream of Oskar in Drosophila germ plasm assembly. *Development* **135**, 1107-1117.

Tanaka, T., Kato, Y., Matsuda, K., Hanyu-Nakamura, K. and Nakamura, A. (2011). Drosophila Mon2 couples Oskar-induced endocytosis with actin remodeling for cortical anchorage of the germ plasm. *Development* **138**, 2523-2532.

Tautz, D. and Pfeifle, C. (1989). A non-radioactive in situ hybridization method for the localization of specific RNAs in Drosophila embryos reveals translational control of the segmentation gene hunchback. *Chromosoma* **98**, 81-85.

Tufail, M. and Takeda, M. (2009). Insect vitellogenin/lipophorin receptors: molecular structures, role in oogenesis, and regulatory mechanisms. *J. Insect Physiol.* **55**, 87-103.

Vanzo, N. F. and Ephrussi, A. (2002). Oskar anchoring restricts pole plasm formation to the posterior of the Drosophila oocyte. *Development* **129**, 3705-3714.

Vanzo, N., Oprins, A., Xanthakis, D., Ephrussi, A. and Rabouille, C. (2007). Stimulation of endocytosis and actin dynamics by Oskar polarizes the Drosophila oocyte. *Dev. Cell* **12**, 543-555.

Verstreken, P., Kjaerulff, O., Lloyd, T. E., Atkinson, R., Zhou, Y., Meinertzhagen, I. A. and Bellen, H. J. (2002). Endophilin mutations block clathrin-mediated endocytosis but not neurotransmitter release. *Cell* **109**, 101-112.

Weibel, E. R. (1969). Stereological principles for morphometry in electron microscopic cytology. *Int. Rev. Cytol.* **26**, 235-302.

Yang, J. S., Zhang, L., Lee, S. Y., Gad, H., Luini, A. and Hsu, V. W. (2006). Key components of the fission machinery are interchangeable. *Nat. Cell Biol.* **8**, 1376-1382.

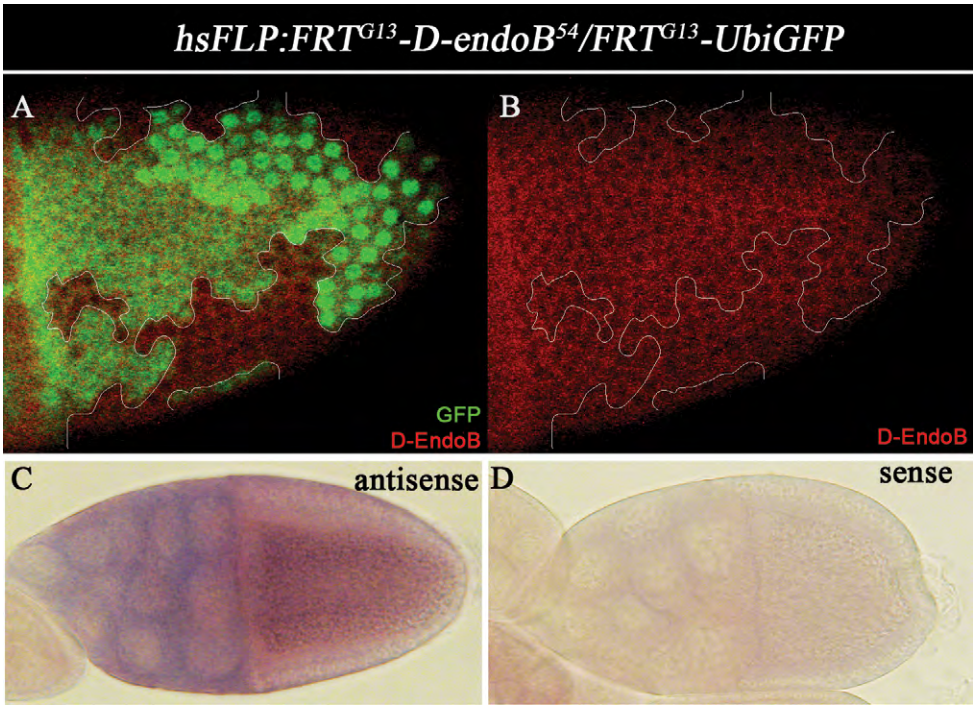

Fig. S1. Verification of D-EndoB mRNA in middle stage egg chambers and protein expression in follicle cells.
(A-B) Mosaic mutant clone analysis show the D-EnodB expression level (red) between wild type (GFP positive) and *D-endoB*^{54} mutant (GFP negative) follicle cells (A). White lines outline the region of clone cells (B). **(C-D)** In situ hybridization of the D-EndoB antisense (C) and sense (D) probe in the wild type middle stage egg chamber.

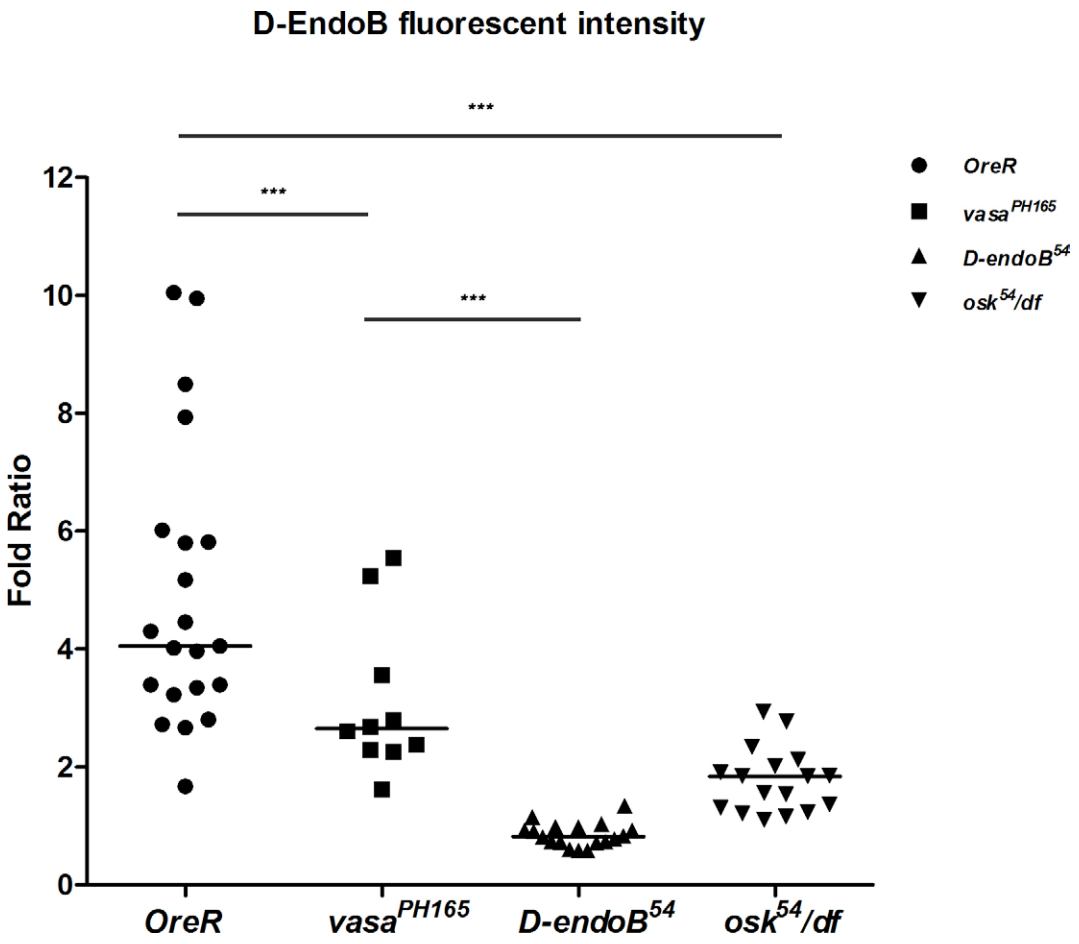

Fig. S2. Quantification of D-EndoB fluorescent intensity at the oocyte posterior.
The fluorescent fold ratio of D-EndoB intensity at the oocyte posterior was measured by Zeiss meta 510. The fold ratio was calculated as the fluorescent intensity in a 5 μm^2 area in the oocyte posterior divided by that in the follicle cell. Note that images of each genotype were selected from Fig. 3. ***P<0.001.

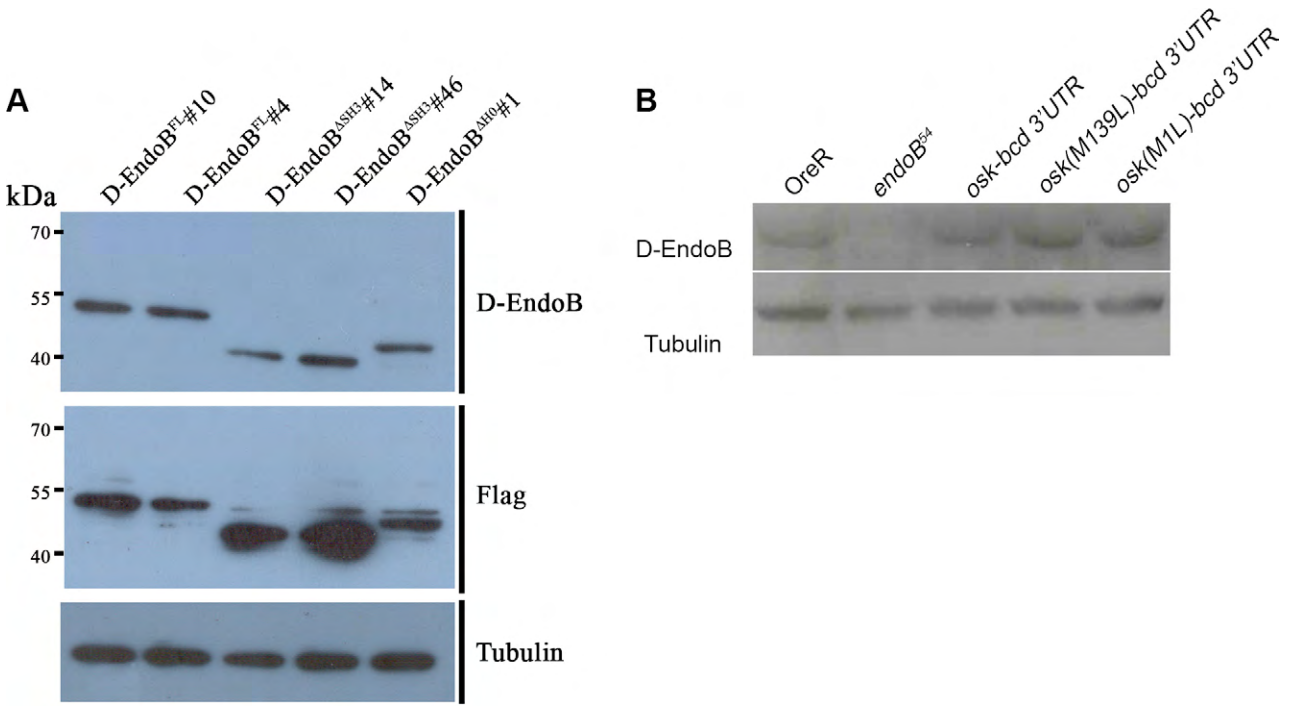

Fig. S3. D-EndoB expression in different transgenic lines.
(A) Flies carried the *UASp D-endoB* transgene, as indicated, were driven by *nanos-GAL4*, and ovaries of each were dissected for protein extraction. The immunoblotting were performed by probing with rabbit ant-D-EndoB, mouse anti-Flag antibody, and mouse anti-Tubulin antibody was the loading control. **(B)** The level of D-EndoB was detected in the ovary lysate of OreR, *D-endoB*^{54} homozygous mutant, *nanos-GAL4* driven *UASp-osk-bcd 3'UTR*, *UASp-osk (M139L)-bcd 3'UTR*, and *UASp-osk (M1L)-bcd 3'UTR* transgenic lines by western blot. Tubulin served as the loading control.

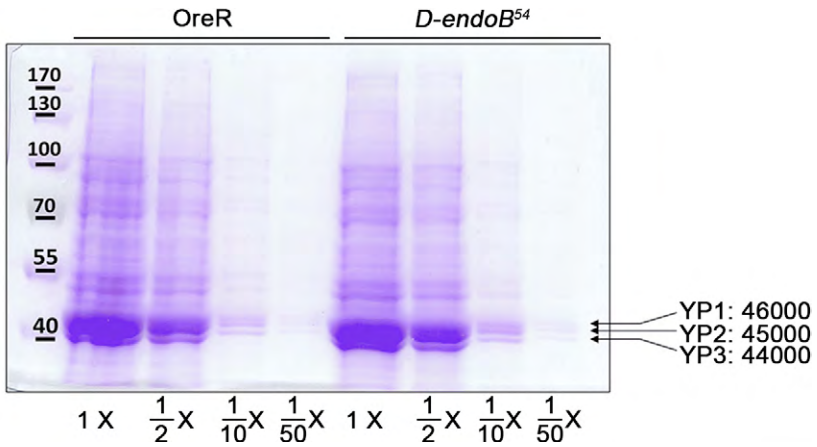

Fig. S4. Detection of Yolk protein levels in wild-type and *D-endoB*^{54} mutant ovaries.
Twenty ovaries from various genotypes were extracted in hemolysis buffer. Each sample was normalized to 7.25 μg/μL followed by series dilution. Samples were then analyzed on a SDS-PAGE and the gel was counterstained with coomassie blue.

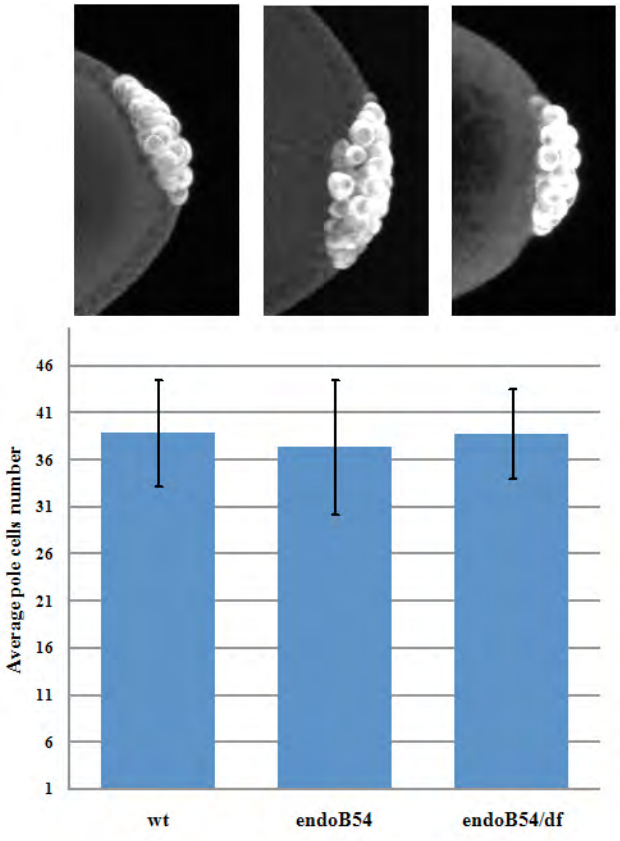

Fig. S5. Determination of pole cell numbers in *D-endoB* mutant embryos.
Stage 3 embryos of each genotype were collected. Following decorionation, the embryos were stain with anti-Vasa antibody to examine pole cells

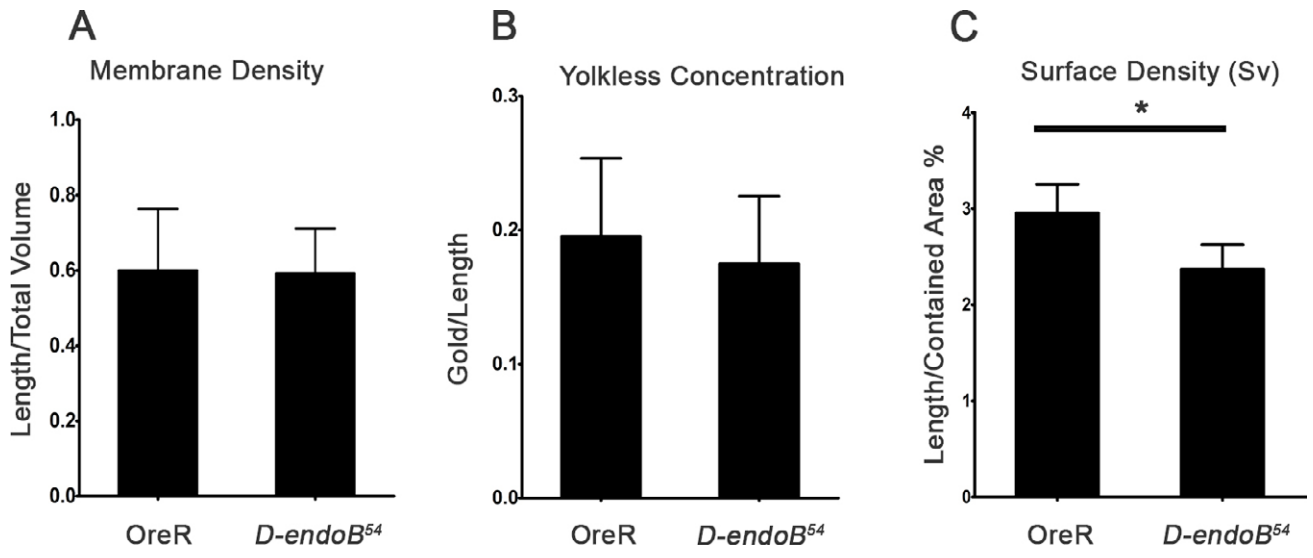

Fig. S6. Surface density of tubulovesicular structures was reduced in *D-endoB* mutant.
(A-B) The tubulovesicular membrane density and its Yolkless concentration were about the same for wild type and the null mutant. Total areas/length/gold scored were 24.2 μm^2/131.8 μm/1011 and 21.9 μm^2/122.6 μm/931 for wild type (n=4) and *D-endoB^{54}* (n=4), respectively. Unit area: 0.0025μm^2; unit length: 0.1μm. **(C)** Surface density of tubulovesicular structures was measured as the ratio of the contour length (intersection counts; I) over the area contained within (points counts; P). Three to four I/P ratio were scored for each animal and analyzed. *, $p < 0.05$.

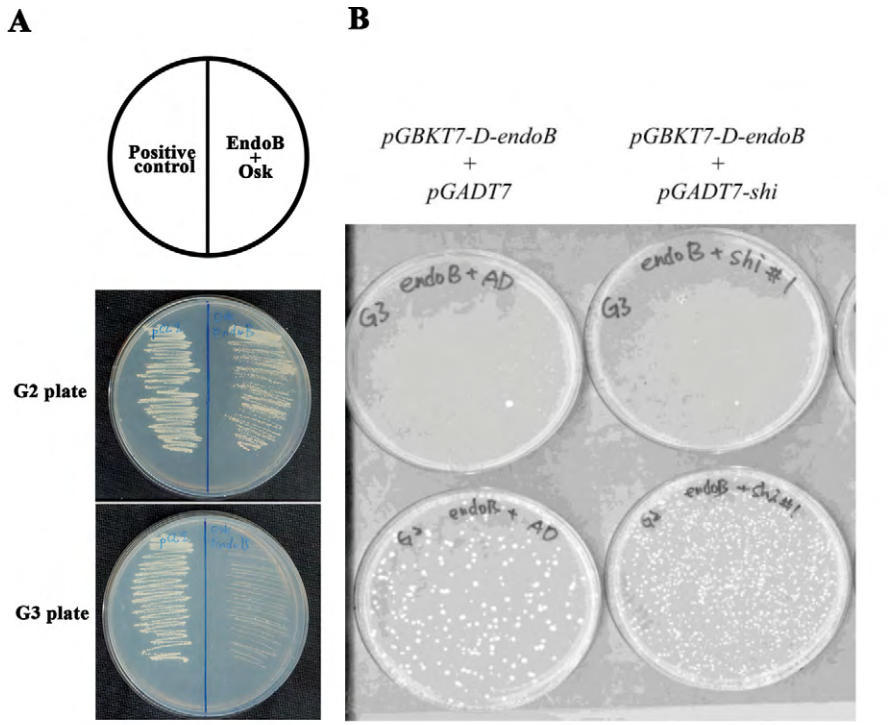

C

	D-EndoB	D-EndoB+Shi	D-EndoB+Oskar
G3 plate	-	-	-
G2 plate	+	+	+

Fig. S7. D-EndoB does not interact with Shibire.
(A-C) Using a yeast two-hybrid system to examine the interaction between D-EndoB, and Oskar (A, C) or Shibere, the *dynamin* homology in *Drosophila* (B, C). The result indicate that D-EndoB does not interact with Oskar or Shibere.

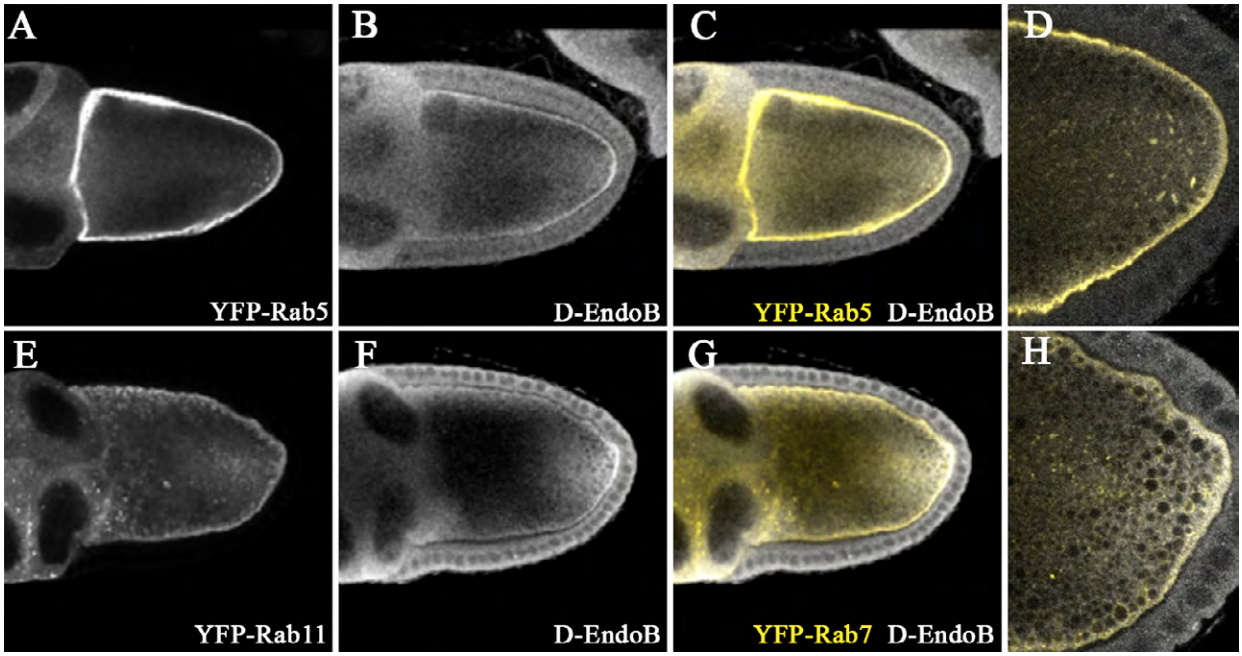

Fig. S8. D-EndoB is co-localized with endosomal protein.
UASp-Rab5-YFP (A-D) and *UASp-Rab7-YFP* (E-H) were expressed by *nanos-GAL4* and were stained with D-EndoB antibody. The expressed endosomal protein (Yellow) was distributed around the oocyte and was colocalized with D-EndoB (White) at the posterior pole. (D, H) Enlargement of the posterior region in the oocyte.